Modelling adaptability: Predictive simulations of STS arm compensation strategies

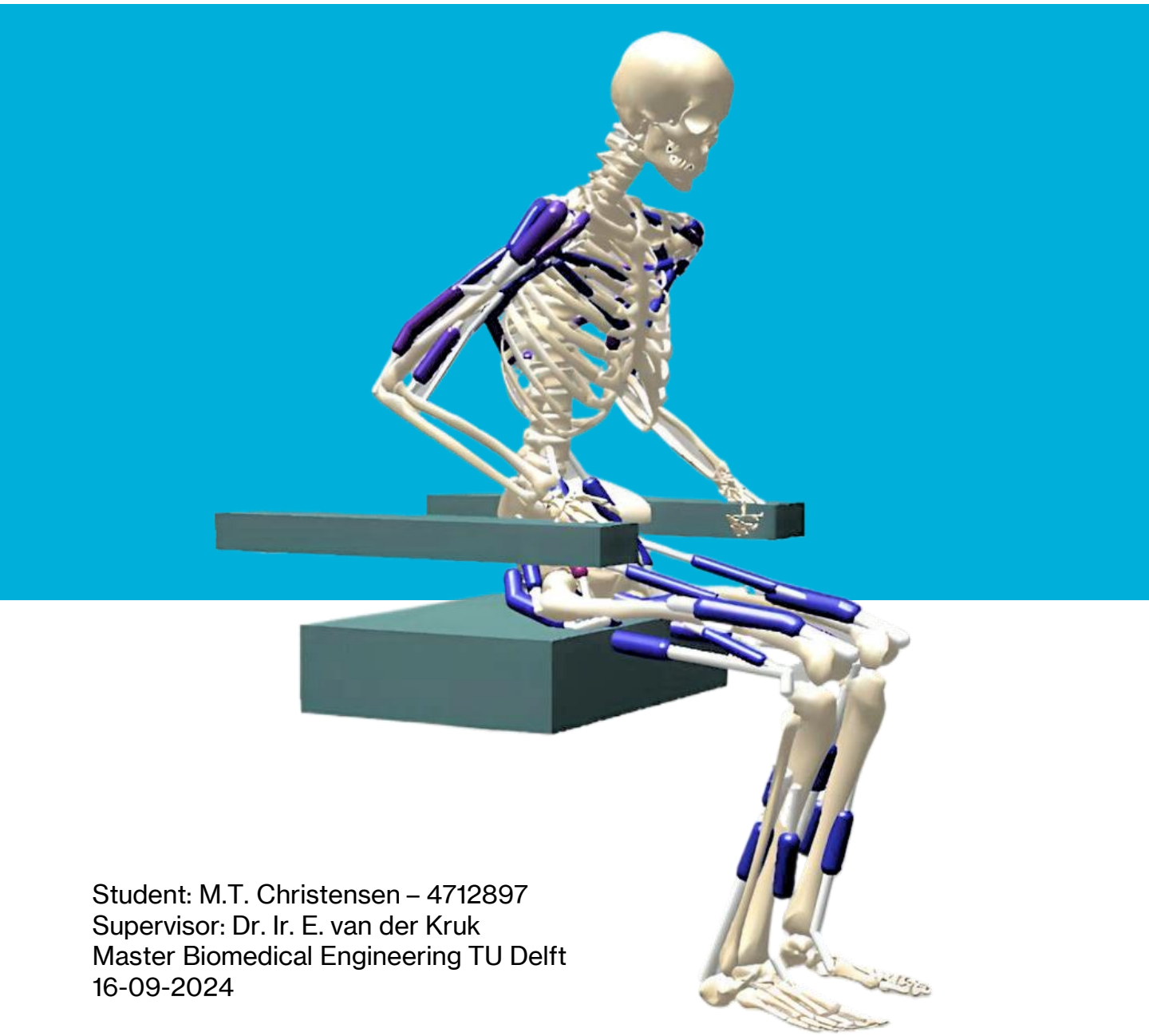

Student: M.T. Christensen – 4712897
Supervisor: Dr. Ir. E. van der Kruk
Master Biomedical Engineering TU Delft
16-09-2024

Abbreviations

General:

Sit-to-Stand	-	STS
Sit-to-Walk	-	STW
Golgi Tendon Organ	-	GTO
Muscle Spindle	-	MS
Osteoarthritis	-	OA
Electromyography	-	EMG
Ground Reaction Force	-	GRF
Degrees Of Freedom	-	dof
Muscle Tendon Unit	-	MTU
Proportional Derivative	-	PD

Strategies:

Arm Swing	-	AS
Armrest Push-off	-	AP
Thigh Push-off	-	TP
Arms Crossed	-	AC

Muscles:

Adductor Magnus	-	AMAG
Gluteus Medius	-	GMED
Iliacus	-	ILIAC
Psoas	-	PSOAS
Gluteus Maximus	-	GMAX
Hamstrings	-	HAM
Biceps Femoris Short Head	-	BFSH
Rectus Femoris	-	RF
Vasti	-	VAS
Gastrocnemius	-	GAS
Soleus	-	SOL
Tibialis Anterior	-	TA
Coracobrachialis	-	CORB
Triceps Longus	-	TRIL
Triceps Lateral Head	-	TRILH
Biceps Longus	-	BICL
Biceps Brevis	-	BICB
Brachialis	-	BRACH
Deltoid	-	DEL
Latissimus Dorsi	-	LATD
Pectoralis Major	-	PECM
Teres Major	-	TERM
Supraspinatus	-	SUPR

1. Abstract
Age-related decline in physical and neural capacity can make the sit-to-stand (STS) motion increasingly difficult for older adults, significantly impacting their quality of life. Despite these declines, humans adopt compensatory movement strategies to mitigate the effects of reduced capacity, maintaining functional mobility. Predictive simulations offer a tool for studying the relationship between capacity decline and compensation strategies. However, previous predictive studies have omitted the modeling and control of arm movements, thus neglecting key arm compensation strategies relevant to the STS motion. Therefore, this study aimed to develop a neuromuscular controller for a three-dimensional musculoskeletal model that includes the arms, enabling the simulation of STS arm compensation strategies. STS arm strategies were successfully simulated and displayed comparable joint kinematics with experimental data. However, the simulations revealed elevated leg muscle activations and an overestimated vertical ground reaction force. Additional simulations with changed conditions demonstrated the effective use of the armrest and thigh push-off strategies to adapt to lower seat heights and reduce peak knee joint load. Overall, the neuromuscular controller in this study provides a new basis for future STS research into uncovering the link between capacity decline and compensation strategies, potentially leading to improved methods for assessing and addressing age-related declines in crucial movements.

2. Introduction
Standing up from a seated position is a critical task in daily life. On average, individuals perform the sit-to-stand (STS) movement approximately 60 times per day [1]. The STS movement is essential for getting out of bed, going to the bathroom or moving between locations. However, routine movements become increasingly challenging with age due to the decline in the physiological abilities of neuromusculoskeletal systems, collectively referred to as "capacity" [2]. The decline in capacity impairs motor control, increasing the risk of falls and overall decreasing the quality of life for older adults [3].

The onset of capacity decline is not immediately noticeable. The human neuromusculoskeletal system exhibits functional redundancy. This allows for the recruitment of alternative muscles or movement trajectories to accomplish the same objective [2]. Furthermore, humans adopt compensation strategies to deal with capacity decline [4]. For instance, during the STS movement, individuals may use their arms for assistance.

The lack of control on measuring the interconnectivity between factors of capacity decline and movement compensation makes understanding their relationship difficult [5]. Indicators of muscular capacity (e.g. muscle mass and strength) and neural capacity (e.g. neural conduction velocity, sensory delays and signal noise) [2] are often captured in isolation [5]. Additionally, there is no way of distinguishing the contributions of individual variables to capacity decline and compensation strategies. However, understanding the link between the decline and compensatory movement could provide insights into the significance of these strategies. This understanding may also facilitate the early detection of capacity decline. It would allow clinicians to intervene earlier to slow the decline or prevent compensatory strategies that could have negative impacts on the body [4].

Predictive simulations may offer a solution for studying the relationship between capacity decline and compensatory strategies. These forward simulations integrate the dynamics of a musculoskeletal model with a neuromuscular controller model that determines the activations of actuators. The resulting movement is optimized according

to an objective function. This method enables the simulation of movements *'de novo'*, without prerecorded movement data, which is not possible with the traditional inverse data-driven approach [6]. Consequently, it allows for the simulation of alternative movements, including those that involve compensatory strategies [6].

Van der Kruk and Geijtenbeek (2024) previously developed and validated a 2D neuromusculoskeletal model combined with a reflex-based controller to simulate the sit-to-walk (STW) movement [7]. The controller, inspired by the work of Geyer and Herr (2010) and Munoz et al. (2022) [8], [9], utilized simple feedback rules that mimicked real-life sensory receptors like the Golgi tendon organs (GTO) and muscle spindles (MS). The simulations in Van der Kruk and Geijtenbeek (2024) [7] demonstrated a high correlation with experimental data and showed the model's ability to adapt to altered conditions, such as lower seat heights or asymmetric foot positioning. Van Minnen (2024) expanded upon this work by adapting the model for the STS scenario and extending it to three dimensions [10], thereby enabling more realistic simulations.

A limitation of previous predictive studies of STS is the absence of arm modelling. The use of arms is particularly crucial for older adults. Mazza et al. (2004) found that nearly half (48%) of a group of healthy elderly participants required the use of their arms to rise from a seat at knee height [11]. Davidson et al. (2013) further showed more than 80 % of people suffering from osteoarthritis (OA) in the knee joints were unable to stand up without the use of arms [12]. Van der Kruk et al. (2021) described three arm strategies found in their literature study frequently used in STS movements, including arm swing (AS), armrest push-off (AP) and thigh push-off (TP) [4]. Trunk flexion momentum, a strategy used by humans to generate additional rising momentum [13], can be aided with additional momentum from swinging the arms. Pushing off on armrests transfers part of the required force from the lower limbs to the arms, alleviating the leg muscles and joints. A study showed 83 % of OA patients using armrest push-off in one or more trials [14], possibly to avoid pain in the knee joints by alleviating the load [15]. Although the biomechanical advantages of the TP strategy are less clear, previous studies have noted its benefits in reducing trunk extension moments and upper limb joint moments in older adults [16, 17].

The AS, AP, and TP strategies have demonstrated significant roles in alleviating the load on the lower limbs and providing assistance during the STS motion. These compensatory strategies are key for older adults to deal with capacity decline, so the role of the arms in simulating STS compensation strategies cannot be overlooked. Therefore, this study aimed to:

Develop a neuromuscular controller for a three-dimensional musculoskeletal model including arms to simulate arm compensation strategies in the sit-to-stand motion

The STS motion with AS, AP and TP strategies were simulated and validated with experimental kinematics, muscle activations (electromyography or EMG) and environmental forces (ground reaction force or GRF, seat force, push-off force). Altogether, the neuromuscular controller in this study provides a new basis for future STS research in studying the relationship between age-related capacity decline and compensatory strategies.

3. Methods

3.1: Musculoskeletal model: MCFB1

The *MCFB1* full-body musculoskeletal model represented a male of height 1.80 m with a mass of 75 kg. The lower limbs and torso were taken from the study of Van Minnen (2024) [10], a three-dimensional adaptation of the *H1120* model by Van der Kruk and Geijtenbeek (2024) [7]. The upper limb model was developed by Thomas Geijtenbeek, adapted from Seth et al. (2019), Van der Helm (1994) and Saul et al. (2014) [18] – [20]. Notably, this newly incorporated upper limb model has not yet been validated or employed in previous studies. The *MCFB1* model was developed as a Hyfydy model to improve the simulation speed [21]. Hyfydy is currently available as a plug-in for SCONE [22], which is an Open Source Software used the for predictive simulations.

The *MCFB1* model contained 26 degrees of freedom (dof) (Figure 1). The 26 dof were comprised of 6 dof joint between the pelvis and the ground (3 translational dof + 3 rotational dof), 3 rotational dof hip joint, 1 rotational dof pin joint in the knee and ankle, 1 rotational dof lumbar joint between the pelvis and the lumbar, 1 rotational dof thoracic joint between the lumbar and the thorax, 3 rotational dof shoulder joint and 1 rotational dof pin joint in the elbows. The forearms and hands were modelled as a single body, simplifying the model by omitting the wrist and radioulnar joints. The forearms were maintained in a constant 90-degree pronated position.

The model was actuated by 52 Hill-type muscle-tendon units (MTUs) [23]. The lower limb MTUs, excluding the adductor magnus (AMAG) and gluteus medius (GMED), were modelled like the *H1120* model from Van der Kruk and Geijtenbeek (2024) [7]. For the muscle properties, the maximal isometric forces (F_{iso}) were adjusted. While the F_{iso} values in the *H1120* model were based on Delp et al. (1990) [24], the optimal fiber lengths (l_O) were derived from the *RAJAG* model by Rajagopal et al. (2016) [25]. In the *MCFB1* model, the l_O values were retained from the *H1120* model, but the F_{iso} values were modified to reflect the F_{iso} / l_O ratio from Delp et al. (1990) [24]. See Appendix A for a detailed calculation of the F_{iso} and values for other leg muscle properties. The AMAG and GMED were added to account for the additional dof of the pelvis [10], with their muscle paths and properties were based on the *RAJAG* model [25]. Similarly to the other lower limb muscles, the F_{iso} were based on the F_{iso} / l_O ratio from Delp et al. (1990) [24].

The upper limb muscles in the model were the coracobrachialis (CORB), triceps longus (TRIL), triceps lateral head (TRILH), biceps longus (BICL), biceps brevis (BICB), brachialis (BRACH), deltoids (DEL1, DEL2, DEL3), pectoralis major (PECM1, PECM2), latissimus dorsi (LATD), teres major (TERM), and supraspinatus (SUPR) (Figure 1).

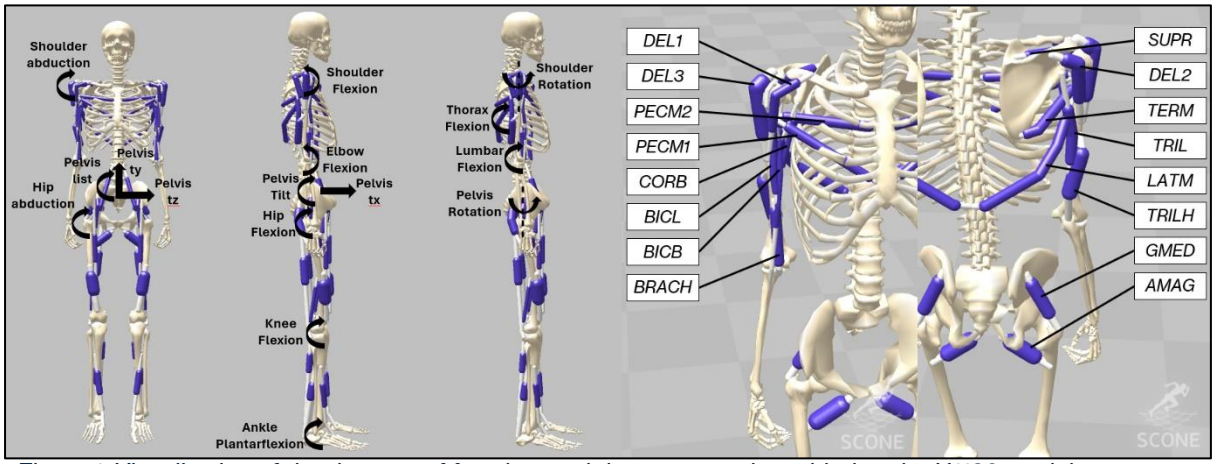

Figure 1: Visualization of the degrees of freedom and the new muscles added to the H1120 model

The properties of these muscles were based on data from Seth et al. (2019) and Saul et al. (2014) [18], [20]. For a detailed description of the arm muscle properties, including their sources, refer to Appendix A. The lumbar and thoracic joints were torque-driven.

Contact points were modelled as Hunt Crossley spheres [26]. Three contact points were placed on the feet: A heel sphere with a radius of 3 cm, and a medial and lateral toe sphere with a radius of 2 cm. A contact point with a radius of 12 cm was placed on the buttocks. Each wrist contained a contact point with a radius of 2 cm. The thighs each contained a contact capsule, with a height of 15 cm and a radius of 6 cm. The rest of the torso and limbs were encapsuled by a contact capsule to prevent other bodies passing through them. The chair seats and armrests were modelled as a box with dimensions 40x12x50 cm and 60x5x10 cm respectively. All body contact spheres and capsules had a plain strain modulus of 17500 N/m^2 and dissipation coefficient of 1 s/m. The chair and armrests had a plane strain modulus of 10000 N/cm and a dissipation coefficient of 2 Ns/m. All contact points had a static friction and dynamic friction coefficients of 0.9 and 0.6 respectively. Joint forces had a limit stiffness of 500 N/m, representing the ligaments.

3.2: Neuromuscular controller

The controller was a reflex-based controller with two states (P1, P2). Each controller state contained the same parameters. The general proprioceptive control equation is described by Equation 1:

$$U = C_0 + K_x(X (t - \delta_t)) \quad (1)$$

Controls were comprised of a constant pre-stimulation (C_0), along with a delayed gain-dependent (K_x) modulation based on feedback from muscle force ($X = F, K_F$), length ($X = L - L_0, K_L$), and contraction velocity feedback ($X = V, K_V$). L_0 is the length-offset, which was set to 1. This approach effectively modelled the proprioceptive sensors found in human muscles. GTOs sense muscle force, while MSs detect muscle length and contraction velocity. The control equation modulated the force of contraction in the original muscle through monosynaptic pathways, or other muscles through antagonistic pathways. The gains were allowed to be both positive and negative. The sign was determined in the optimization. Finally, muscles received feedback from the pelvis tilt to mimic vestibular senses. The vestibular feedback, along with the lumbar and thoracic joints motor torque, were proportional derivative (PD) controlled. Control was based on the deviation from a target angle, controlled by the current angle and angular velocity of the corresponding joint.

δ_t were the time delays related to the neural latencies. Lower limb delays were based on Van der Kruk and Geijtenbeek (2024) [7]. The time delays were implemented in multiples of 5 ms and were based on the distance of the muscles to the spine. Muscles affecting the hip joint were set to 10 ms, the knee joint 20 ms and the ankle joint 35 ms. An exception were the hamstrings (HAM), set to a monosynaptic delay of 15 ms. A similar trend in time delays was used for the upper limb muscles. Muscles affecting the shoulder joint were set to 10 ms, like for the hip joint. Muscles affecting the elbow joint were set to 15 ms. This was deliberately 5 ms quicker compared to the knee joint, to account for the shorter length of the upper arm compared to the upper leg. The vestibular time delays were matched to the leg muscle time delays. For proximal arm muscles this was 40 ms and for distal arm muscles this was 45 ms. Table 1 shows an overview of the time delays.

In total, the controller contained 1033 free parameters for optimization. This included the controller gains and pre-activation, the target angle for the pelvis, lumbar and thoracic joints, and the transition time between the controller states.

3.3: Initial positions and conditions

In this study, three arm compensation strategies were analysed:

- Arm swing (= AS)
- Armrest push-off (= AP)
- Thigh push-off (= TP)

Additionally, a baseline condition where the arms were not utilized, termed the Arms Crossed (AC) strategy, was simulated by keeping the arms crossed on the chest. Initial positions were based on the average starting positions of participants from a subset of kinematic data from Van der Kruk et al. (2022) [5]. The shoulder and elbow joints were given an additional offset to ensure contact with the armrests and thighs in the AP and TP strategies, respectively. The humerus was internally rotated compared to the thorax by 30 degrees, and the forearm was extended compared to the humerus by 30 degrees. For the AC strategy, the arm angles were guessed to portray the crossing of the arms kept close to the chest. Van der Kruk et al. (2022) [5] excluded the AC strategy, so the remaining angles of the initial position were equal to AS initial position. The velocities of the skeletal bodies and joints were initially set to 0. Initial values for the controller variables, were taken from Van der Kruk and Geijtenbeek (2024) [7]. Adjustments were made for the gluteus maximus (GMAX) and vasti (VAS) muscles, which displayed persistent maximal activation during parts of the simulation. To address this, the monosynaptic feedback gains and pre-activation levels for the GMAX muscles were halved. For the VAS muscles, feedback gains and pre-activation were minimized to 0.01. For the upper limb muscles, feedback gains and pre-activations were uniformly set to 0.2.

Table 1: Neural latencies of monosynaptic, antagonistic and vestibular pathways

Lower limb/torso:	Mono-synaptic delay	Antagonist	Antagonist delay	Vestibular delay	Upper limb:	Mono-synaptic delay	Antagonist	Antagonist delay	Vestibular delay
GMED	10	AMAG	10	40	**CORB**	10	-	-	40
AMAG	10	GMED	10	40	**TRIL**	10	BICL, BICB, BRACH	10	40
ILIAC	10	GMAX	10	40	**TRILH**	15	BICL, BICB, BRACH	15	45
PSOAS	10	GMAX	10	40	**BICL**	10	TRIL, TRILH	10	40
GMAX	10	ILIAC, PSOAS	10	40	**BICB**	10	TRIL, TRILH	10	40
HAM	15	RF, VAS	20	45	**BRACH**	15	TRIL, TRILH	15	45
BFSH	20	RF, VAS	20	45	**DEL1**	10	PECM1, PECM2, LATD, SUPR, TERM	10	40
RF	20	HAM, BFSH	20	45	**DEL2**	10	PECM1, PECM2, LATD	10	40
VAS	20	HAM, BFSH	20	45	**DEL3**	10	PECM1, PECM2, LATD, SUPR, TERM	10	40
GAS	35	TA	35	55	**LATD**	10	DEL1, DEL2, DEL3, SUPR	10	40
SOL	35	TA	35	55	**PECM1**	10	DEL1, DEL2, DEL3, SUPR	10	40
TA	35	GAS, SOL	35	55	**PECM2**	10	DEL1, DEL2, DEL3, SUPR	10	40
Lumbar				35	**TERM**	10	DEL1, DEL3	10	40
Thoracic				30	**SUPR**	10	PECM1, PECM2, DEL1, DEL3, LATD	10	40

3.4: Simulation framework

Simulations were done in the SCONE software [22]. Simulation time was set to 3 s and stopped if the time was met or if the COM height fell below 0.8 m after 1.5 s of the simulation. A set of objective measures were determined and minimized in the optimization.

- *Height measure;* The pelvis height was set to be at least 0.88 m at 1.5 s of the simulation, to ensure the model would stand up and stay standing. This measure was set to zero if the height was achieved and kept after 1.5 s
- *Range measures;* Certain dof were bound to specific joint angle ranges, to penalize excessive range of motion from ligaments, soft tissue and joint geometry that were not modelled. These included the lumbar extension (-50...30 degrees), thorax extension (-15...15 degrees), pelvis tilt (-50...30 degrees) and ankle angle (-60...60 degrees). These measures were set to zero if the joint angles were in range.
- *Effort measures:* This ensured the simulations would be performed with the least effort, similar to how the central nervous system optimizes movement to minimize energy consumption [6]. These measures were the only non-zero term in all final runs of the simulations. Effort measures included the cubed muscle activation, the motor torque of the lumbar and thoracic joints and the metabolic energy expenditure based on Wang et al. (2012) [27]. The metabolic energy expenditure was defined as the sum of the muscle activation rate, the muscle maintenance heat rate, the muscle shortening heat rate, and the positive mechanical work rate.

Additional range measures were added to the arm joints to increase the speed of finding solutions in the initial simulations. The extra measures were removed in subsequent runs to allow the optimization to find the optimal solution freely. The AC simulation was herein an exception. The extra range measures were necessary to keep the arms in a crossed state. Optimization was performed using the Covariance Matrix Adaptation Evolutionary Strategy (CMA-329 ES), with a population size for each generation of 10. The number of iterations was dependent on the simulation time. Each strategy was optimized with multiple parallel runs with the same initial guess. Subsequent optimizations were performed with the best previous result.

3.5: Validation

To validate the simulations, a subset of kinematic and kinetic data was taken from van der Kruk et al. (2022) [5]. In their study, kinematic and kinetic data of STS was recorded of young (27.2±4.6 years, N = 27, 14 F) and older (75.9±6.3 years, N = 23, 12 F) adults. Participants were seated on an instrumented chair with armrests, which was adjusted in height to have an approximate 90 degrees knee angle while seated in neutral position. The STS movement was performed at self-selected pace and as-fast-as-possible each with 3 repetitions. Strategies recorded included the arm swing, thigh push-off and armrest push-off. Reaction forces were measured via two Kistler force plates embedded in the walkway, one at the seat and two 9129 AA Kistler force plates in the armrests. A Vicon system with 10 cameras (MX T20) captured the STS volume (100 Hz). Participants were equipped with 84 reflective markers. As the *MCFB1* model used in the simulations was based on a young male adult, 8 participants of the young male adults were included in the verification.

Marker trajectories and GRFs were translated into joint kinematics and kinetics through inverse kinematics and dynamics in OpenSim 4.2, using the musculoskeletal model of Rajagopal et al. (2016) [25]. Muscle activations were compared to EMG data. The EMG data was high pass filtered, rectified and low pass filtered with a 20 Hz cut-off frequency. Because the maximal voluntary contraction was not measured, the EMG data was normalized to the maximal EMG measured per participant over all trials. This could result in overestimated simulated activations compared to the EMG data.

Simulations were verified by comparing time-normalized joint angles, muscle activations and environmental forces. Additionally for the AP and TP simulations, the push-off forces over time were compared. All graphs contained the simulated data, mean experimental data, and the minimal and maximal values measured across all participants. Because the dataset excluded the AC strategy, data from Caruthers et al. (2016) [28] was compared to the AC simulation to give an indication of the validity of the simulation. Specifically, the hip, knee and ankle joint moments over time obtained through inverse dynamics, as well as maximal muscle forces throughout the motion obtained through static optimization were compared.

3.6: Exploring adaptational capabilities

To demonstrate the model's adaptability, two modifications were introduced to the controller. Firstly, the seat height was reduced by 10 cm. New simulations were conducted with this configuration for each strategy. Initial positions were adjusted for the lowered seat height. Secondly, an additional penalty measure was incorporated to penalize knee joint load. This mimicked the way OA patients would relieve the pain in their knee joints. New simulations were performed with the additional knee joint load penalty. Specific variables between the original, lower seat height, and unloaded knee joint simulations were compared:

- The lumbar extension moment to analyze the ability of TP strategy to alleviate the lower back moment
- The GMAX/VAS activations and GRF to analyze the leg efforts in rising up. The GMAX and VAS muscles were shown to be the biggest contributors in the simulation. Furthermore, in testing the lower seat heights, the simulations displayed an increase in activation mainly for the GMAX and VAS muscles.
- The peak push-off forces to analyze the use of the arms in the compensation strategies
- Total metabolic energy expenditure to determine the effort required to rise up in different conditions. This was defined as the metabolic energy consumed as in Wang et al. (2012) [27] over the duration of the STS motion in Joule.
- The peak knee joint load to determine the effectiveness of the unloading of the knees. The knee joint load was defined as the reaction force vector of all forces applied to the knee in bodyweight (BW).

Results

4.1: Simulation and verification of STS arm strategies

All arm strategies were successfully simulated, with their motions illustrated in Figure 2. The AS, AP and TP arm strategies were analyzed in terms of joint angles (Figure 3), muscle activations (Figure 4), and environmental forces (Figure 5). Simulation data (red dotted lines) was compared to the mean experimental data (black lines) and the minimal/maximal

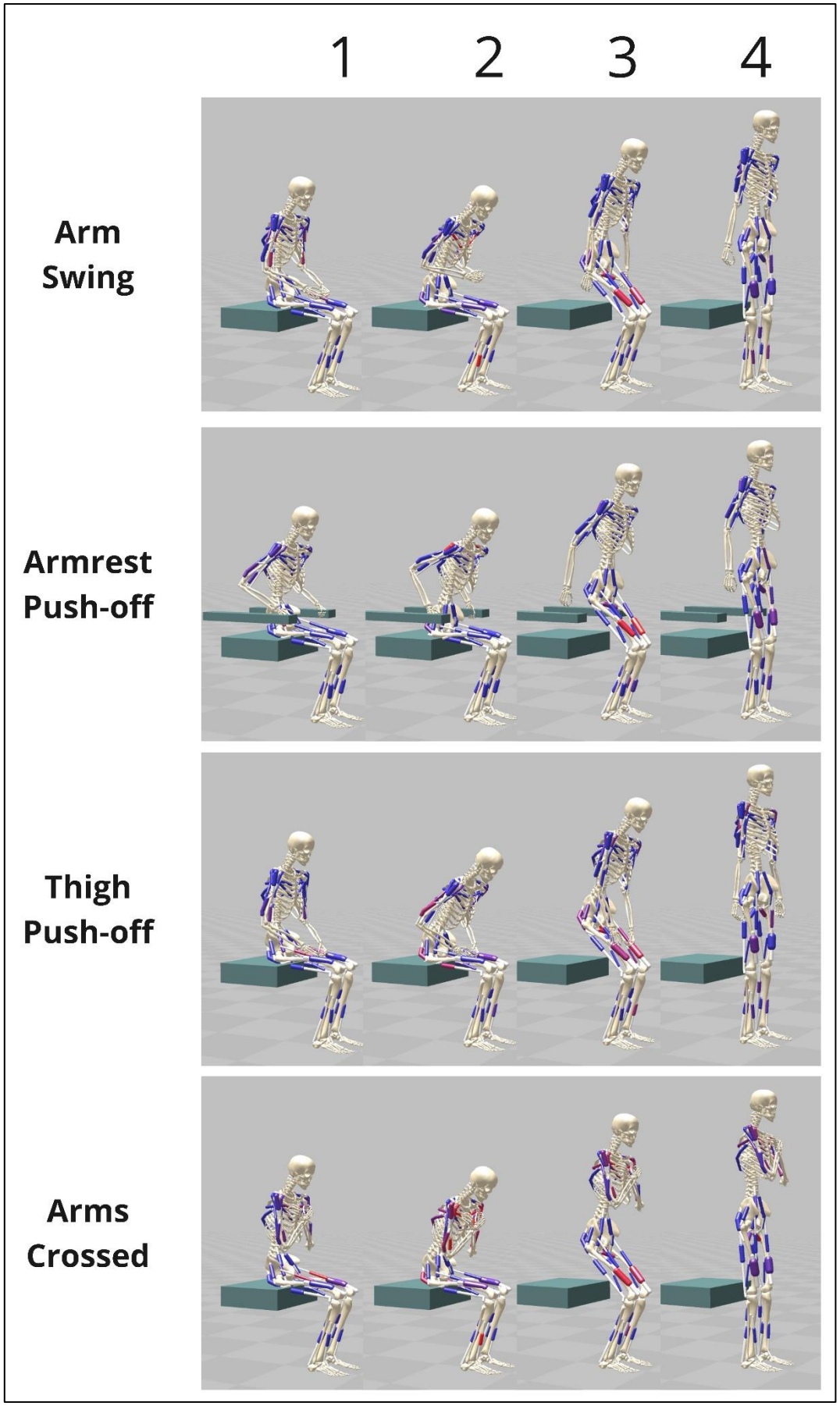

Figure 2: Visualizations of the four arm compensation strategy simulations; 1: Initial position, 2: State transition (ST), 3: 50% motion, 4: Final position

values measured across all participants (grey hue). The STS motion was normalized over time from 0% and 100%, representing the start and end of the motion.

The kinematics of the AS, AP, and TP simulations generally matched experimental STS data (Figure 3), although some deviations were noted. The pelvis tilt and lumbar extension in the AP simulation fell outside the experimental range towards the end of the motion. Additionally, the AP lumbar joint started extending earlier in the motion. The AP shoulders remained extended from 50% STS motion, falling outside the experimental range. The TP shoulders showed greater adduction around 50% motion compared to the experimental data. As mentioned in the Methods, the shoulder rotation and elbow flexion initial angles were offset. Consequently, the TP shoulder rotation and the elbow flexion angles of each strategy fell outside the observed range. For an extensive analysis of the joint kinematics, including lower limb angles, see Appendix B - E.

The simulated muscle activations were generally overestimated compared to the mean measured EMG data, particularly for the HAM, VAS and GMAX muscles (Figure 4). Nevertheless, the HAM, VAS and GMAX peaks of the simulated muscle activations generally complied with the peaks in the mean EMG data and maximal measured range of EMG data. However, the HAM and GMAX muscles deactivated after 50% of the STS motion in the simulation, contrasting with their continued activation in the experimental data. Furthermore, the RF, GAS and SOL muscles showed minimal activation in the simulations despite being active in the EMG data.

Figure 5 illustrates the interaction forces between the model and the environment. Both simulated and experimental vertical GRF followed similar trends, consistent with other studies [29, 30]. However, the simulated peak vertical GRF was higher than the experimental peak at seat-off in the AS and TP simulations. Simulated and the maximal measured peak vertical GRF (1.5 – 1.6 N/BW) were generally higher compared to other studies (1.2 – 1.3 N/BW) [29, 30]. Overestimated simulated vertical GRF may be caused increased VAS and GMAX activation, leading to larger knee and hip extension moments

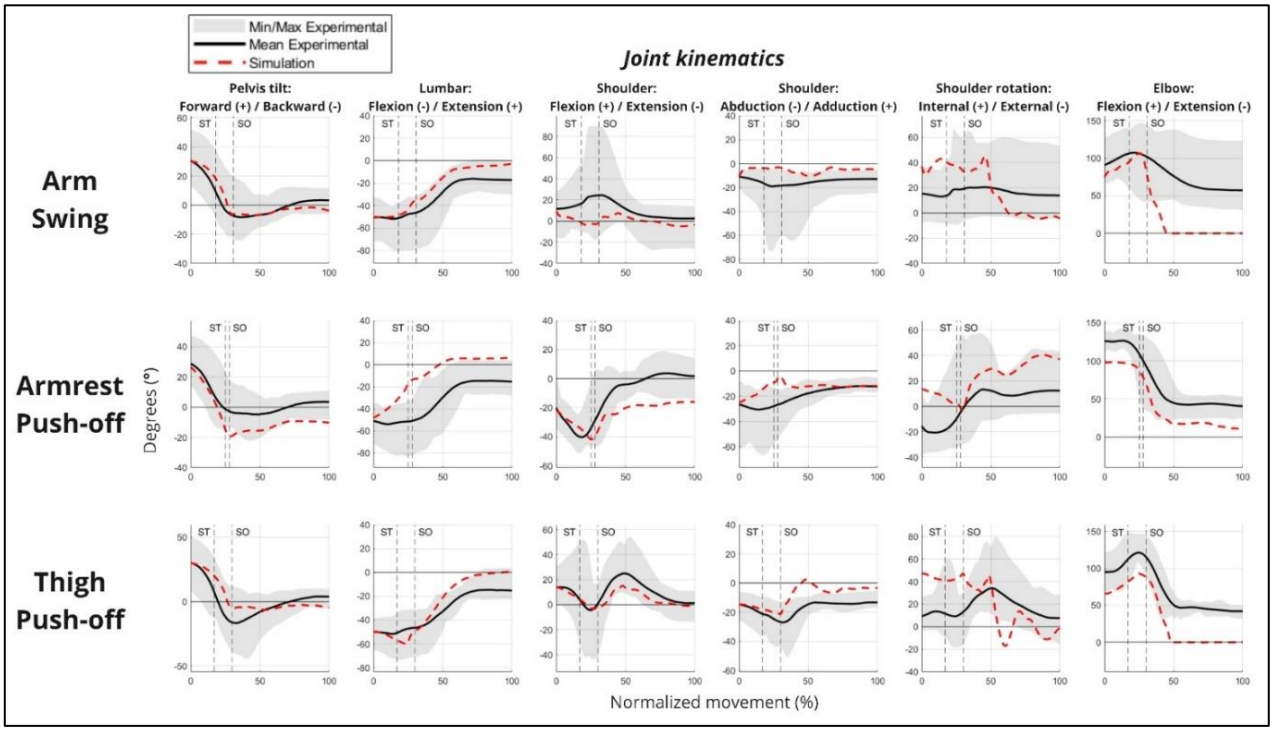

Figure 3: Right-sided joint angle verification between simulated and experimental joint angles. Simulated angles shown as red striped line, experimental angles shown as black line with minimal and maximal range of motion measured; Data was normalized over the duration of the STS movement. ST = State Transition, SO = Seat Off

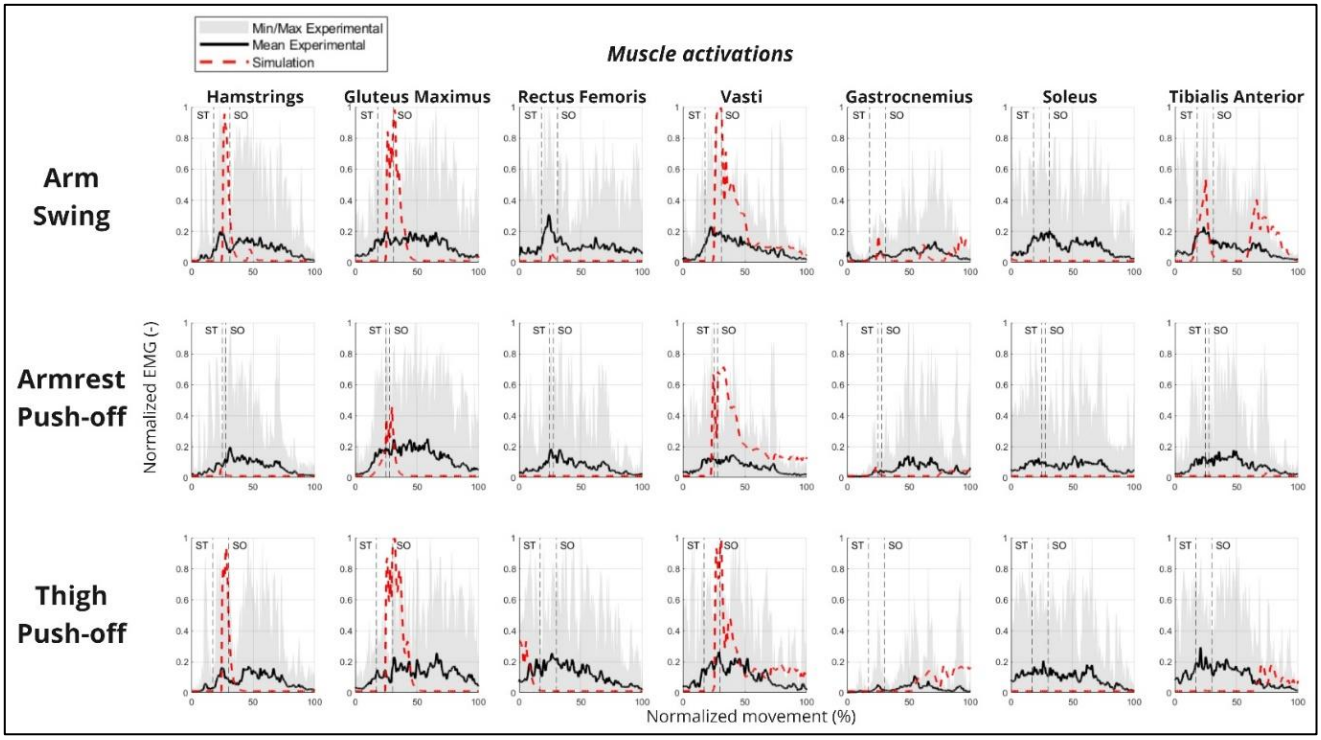

Figure 4: Right-sided muscle activation verification between simulated activations and experimental EMG data. Simulated activation shown as red striped line, experimental EMG as a black line with minimal and maximal range of motion measured. Data was normalized over the duration of the STS movement. ST = State Transition, SO = Seat Off

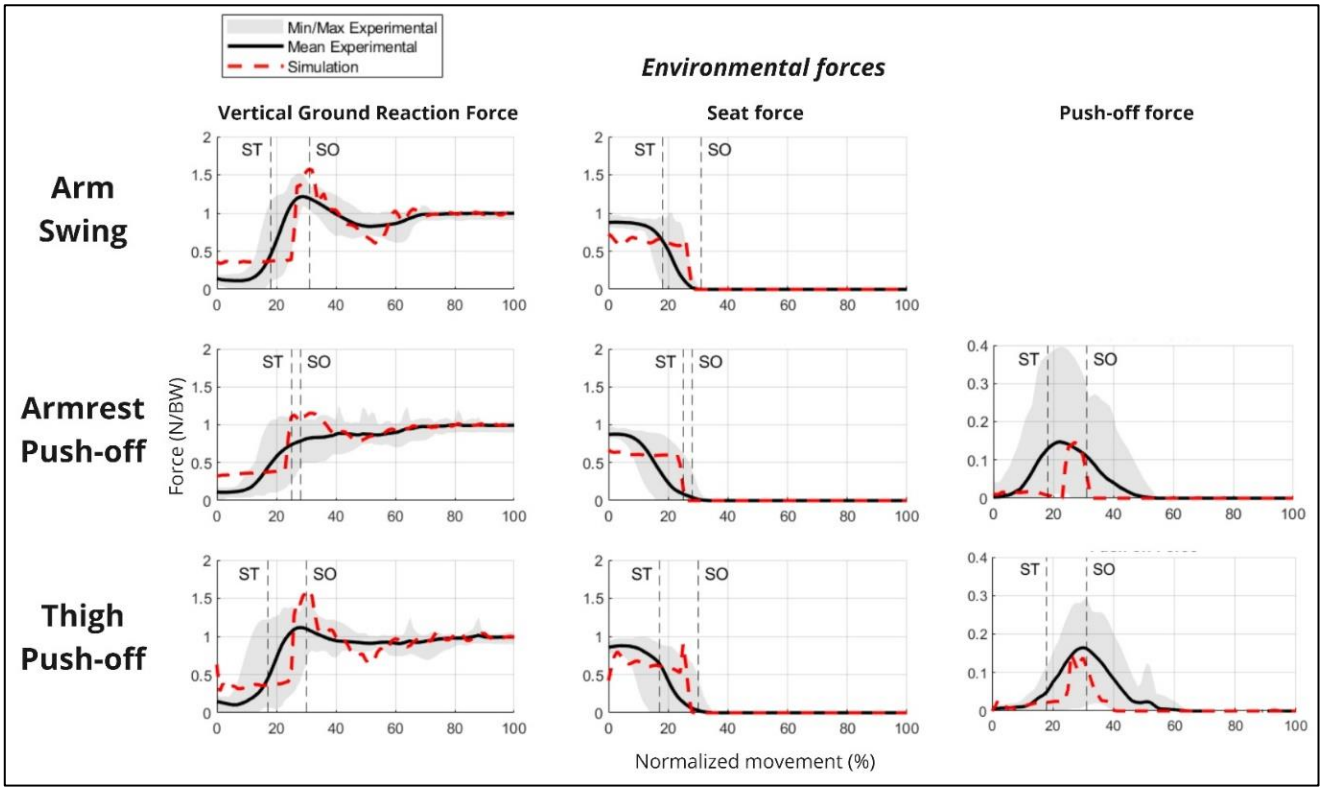

Figure 5: Environmental force verification between simulated and experimental. Simulated force shown as red striped line, experimental force shown with minimal and maximal range of motion measured.; Ground reaction force taken as a sum of both legs. Push-off force is an average of both arms. Data was normalized over the duration of the STS movement. ST = State Transition, SO = Seat Off

and, consequently, a greater downward force. Furthermore, the experimental data displayed a smooth transition from 1 N/BW to 0 N/BW, indicating a gradual rising motion. In contrast, the simulated seat force showed a more abrupt transition. The push-off forces for the AP and TP simulations fell within the experimental range. Both strategies had peak push-off forces near the experimental mean but with shorter push-off durations compared to experimental observations.

The AC strategy was compared to data from Caruthers et al. (2016) [28]. Figure 6 shows the hip, knee and ankle joint moments during the STS motion obtained through inverse dynamics. The trends in the simulation were similar to experimental data, with both showing extension moments at the hip and knee, and plantarflexion at the ankle. Table 2 shows the mean maximal force throughout three phases of the STS motion of a subset of muscles from Caruthers et al. (2016) [28]. Simulated peak muscle forces generally showed similar order of magnitudes and fell within one standard deviation, except for the RF muscle, which was outside this range.

4.2: Simulation of arm compensation strategies in modified conditions

The results of the simulations with modified conditions compared to the original simulations are shown in Figure 7. Table 3 additionally presents the metabolic expenditure defined as in Wang (2012) [27], the peak push-off force for the AP and TP simulations, and the peak knee joint load. The average simulated metabolic expenditure was 1158 J. For reference, a single STS transition for healthy adults has been shown to require 0.33 kcal or 1381 J using indirect calorimetry [31]. The simulated peak knee joint loads ranged from

Table 2: Maximum muscle forces comparison between the AC simulation and Caruthers et al. (2016) [28]. Peak force determined as mean of three STS phases, with one standard deviation

Muscle	Maximum Muscle Force Caruthers et al. (2016); (N)	Maximum Muscle Force AC simulation (N)
GMAX	2009 ± 277.3	1800
RF	944.0 ± 382.2	483.5
VAS	2984.0 ± 559.5	3496
SOL	460.6 ± 213.3	547.3

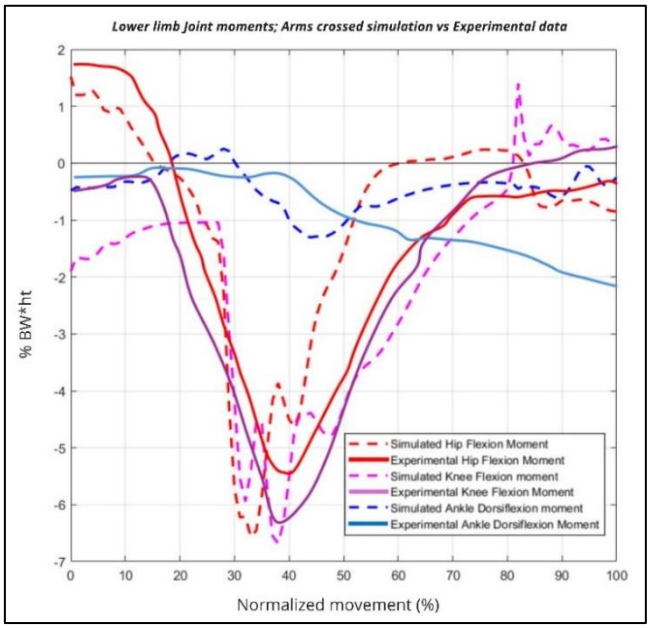

Figure 6: Right-sided lower limb joint moments; comparison between AC simulation and Caruthers et al. (2016). Experimental joint moments obtained through inverse dynamics.

2.93 – 7.81 BW. Peak knee joint load has been shown to range between 2 – 5 BW in STS. The original simulations and low seat height simulations peak knee joint load surpassed the measured range [32].

The AC strategy required a significantly higher metabolic cost when rising from a lower seat, with an increase of 628 J (53%) (Table 3) compared to the original simulation. This increase was linked to heightened activation of the GMAX and VAS muscles (Figure 7), both of which reached a plateau of maximal activation near the seat-off point. In contrast, the AC unloaded knees simulation showed a similar metabolic expenditure to the original simulation but resulted in a decrease in peak knee joint load by 2.61 BW (22%) (Table 3).

The AS strategy also showed an increase in metabolic expenditure when rising from a low seat, with a rise of 520.4 J (56%) (Table 3). Like the AC strategy, this was accompanied by maximal activation plateaus in the GMAX and VAS muscles (Figure 7). However, the AS strategy effectively reduced the peak knee joint load by 3.43 BW (49%) (Table 3) and lowered both VAS activation and the peak vertical GRF compared to the original simulations (Figure 7).

Using the AP strategy, the model managed to rise from a lower seat with an increase in metabolic expenditure of 360.4 J (41%), which was lower than the increase observed with the AC strategy. VAS muscle activation was slightly higher compared to the original simulation, but other variables remained similar. The peak push-off force and push-off duration both increased. The AP strategy, which already showed the lowest knee joint load of 4.25 BW in the original simulation, further reduced the peak knee joint load by 1.32 BW (31%). The total lumbar extension moment, GMAX activation, VAS activation, and peak vertical GRF were all lower than in the original simulation.

The TP strategy allowed the model to rise from a lower seat with a smaller increase in metabolic expenditure of 232.5 J (23%). This was accompanied by an increase in both peak push-off force and push-off duration. The GMAX muscle activation was lower compared to the original simulation. The TP strategy was effective in unloading the knees, reducing the knee joint load by 3.37 BW (49%). The VAS muscle showed overall lower activation, and the push-off force and duration remained similar to the original simulation.

5. Discussion

5.1: Discussion and conclusions

The goal of this study was to develop a neuromuscular controller for a three-dimensional musculoskeletal model that included arms, capable of predictively simulating sit-to-stand strategies using arm movements. The simulations showed that the model used its arms in a way similar to humans, as the resulting STS-kinematics were comparable to experimental data. Still, the simulations displayed both over- and underestimated muscle activations, accompanied by overestimated peak vertical GRF. Validating the simulations also revealed if the arm strategies were effectively used.

In the AS strategy, the simulated shoulder initially extended, while the experimental shoulder flexed. Since shoulder extension would counteract the desired forward momentum of an arm swing, this difference indicated that the AS strategy might not have been fully utilized in the simulation. High activations in the VAS and GMAX muscles were also observed, along with an overestimated GRF at seat-off, likely due to the increased hip and knee extensor moments. These findings suggest that the AS strategy relied heavily on the legs to stand up, underutilizing the arms.

Table 3: Comparing quantitative variables across simulations with changed conditions

	Metabolic expenditure (J)			Peak push-off force (N/BW)			Peak knee joint load (BW)		
	Original	Low seat height	Unloaded knees	Original	Low seat height	Unloaded knees	Original	Low seat height	Unloaded knees
AC	1192	1820	1198	-	-	-	6.01	7.27	4.66
AS	923.6	1444	1023	-	-	-	7.04	7.50	3.61
AP	879.6	1240	940.2	0.130	0.238	0.176	4.25	4.85	2.93
TP	989.5	1222	1022	0.145	0.278	0.155	6.90	7.81	3.53

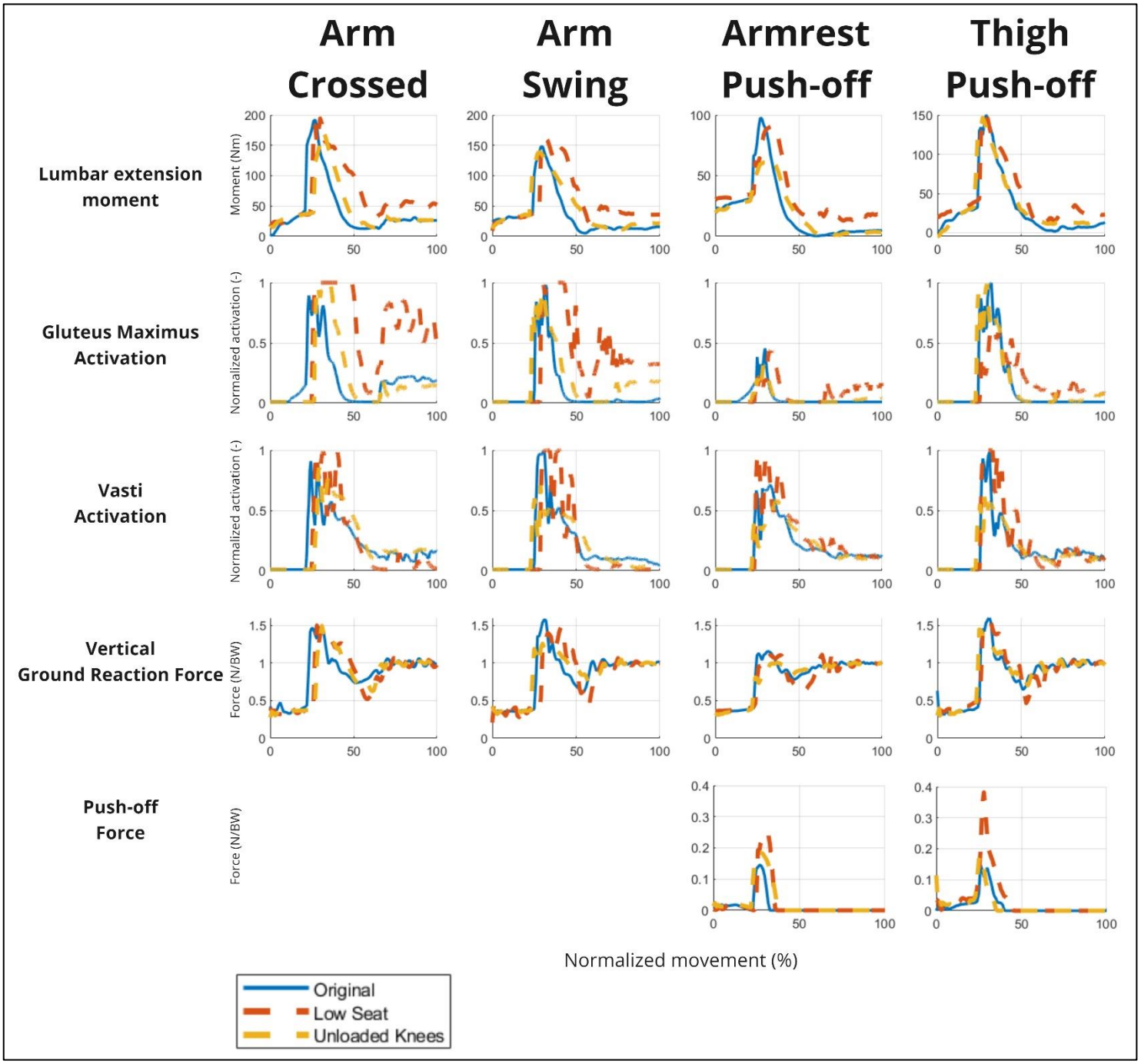

Figure 7: Comparing important variables across simulations with changed conditions. Right-sided muscle activation taken, GRF and push-off force were dual-sided.

The effectiveness of the TP strategy was less obvious. Like the AS simulation, the TP simulation exhibited high VAS and GMAX activations, with an overestimated vertical GRF at seat-off. Additionally, the push-off force duration was shorter than in the experimental data, indicating underutilization of the TP strategy. However, the TP strategy did show a functional effect, reducing the lumbar extension moment by approximately 50 Nm compared to the AC strategy (Figure 7). This was consistent with previous studies that suggested thigh push-offs help reduce trunk extension moments [16][17].

The AP strategy demonstrated the lowest leg muscle activations among the strategies, and the simulated vertical GRF fell within the measured range. Although the mean experimental vertical GRF did not peak above 1 N/BW like in the simulation, the simulation showed a similar trend to previous findings by Etnyre and Thomas (2007) [29]. The reduced leg muscle activations and realistic GRF trends indicated that the AP strategy was effectively used. However, like with the TP strategy, the duration of push-off force was shorter in the simulation than experimentally observed.

The simplified modelling of the hand contact points and wrist dof's can be attributed to this. The contact points were modelled as a single sphere near the base of the palm. This limited force application to that area and did not allow for gripping the armrests. Furthermore, the forearm was modelled as one body, meaning the wrist had no dof's. Humans are able to distribute the load across the palms of their hands, while also rolling off from the arm rests or thighs with the additional dof's of the wrist joint. The simplified modelling of the hand and contact did not allow for the force distribution or roll-off, causing the push-off force to only be applied for a short duration.

Despite the limitations, the simulation displayed realistic kinematics and push-off forces within the measured range. While the AS strategy seemed underutilized, both the AP and TP strategies were shown to be effective.

The model's ability to adapt to altered conditions through arm strategies was also tested to demonstrate not only human-like motion but also the capacity to adjust to varying scenarios.

Without using arms (AC), the model required significantly more effort to rise from a lower seat, but was able to reduce the knee load. In contrast, the AP and TP strategies enabled rising from a lower seat and alleviating knee load with a relatively smaller increase in metabolic expenditure compared to the AC strategy. Both the AP and TP simulations showed higher peak push-off forces under altered conditions. The AP strategy allowed the model to rise from a low seat with a slight increase in VAS activation, while the AC strategy demanded increased, high activations from both the GMAX and VAS muscles. The TP simulations generally exhibited lower lumbar extension moments compared to the AC strategy. Despite similar lumbar extension moments across different conditions, the TP strategy more effectively reduced knee load than the AC strategy, suggesting potential additional benefits or mechanisms to the TP strategy not explored in this study.

The AS strategy offered advantages over the AC strategy, such as lower metabolic expenditure in the original AS simulation compared to the AC simulation. However, it is important to note that the AC strategy required additional effort to maintain the arms in a crossed position, with the AC strategy using 393.8 J in the arms and the AS strategy using 113.8 J. Therefore, Both strategies demanded similar effort from the legs, with no significant advantage observed in the AS strategy under lower seat conditions. In the AS unloaded knee simulation, the AS strategy did manage to reduce peak knee joint load compared to the AC simulation, though the mechanism behind this reduction remains unclear.

Overall, the model, controller, and simulation framework effectively predicted realistic STS motions and demonstrated the ability to adapt to changing conditions, particularly through the effective use of the AP and TP arm strategies.

5.2: Limitations

Several limitations in this study should be noted. The controller is currently robust specifically for the *MCFB1* model. Throughout the study, new insights led to minor adjustments in the maximal isometric forces. This made it difficult to achieve stable standing solutions in subsequent simulations, despite having found stable solutions prior to the changes. Even when stable solutions were identified, multiple muscles displayed undesirable plateaus of maximal activation. This limit is set manually, so the final simulation might not reflect the actual activations the controller could have achieved. The controller required manual tuning of reflex controls and initial monosynaptic and antagonistic feedback gains to reduce muscle activations and produce acceptable simulations. Even then, the current low seat simulations from the AC and AS strategies still showed GMAX and VAS activations plateauing at maximal activation.

Furthermore, the shoulder rotation and elbow flexion angles exhibited similar trends to the experimental data, but were offset by approximately 30 degrees. This offset was intentionally set to achieve an initial position capable of effective push-off on the armrests and thighs. Without this adjustment, the arms would not align with the armrests or thighs. When visually comparing the *MCFB1* model to the *RAJAG* model utilized in the experimental analysis (Figure 8), a noticeable offset in joint angles was evident. Initial assumptions suggested that differences in Euler angle definitions between *SCONE* (used in this study) and *OpenSim* (used for the *RAJAG* model) might be responsible for this offset, but this hypothesis was not supported. Additionally, Wu et al. (2005) described two methods for defining the rotational center of the shoulder joint [33]. It was possible that differences in the definition of the rotation center between *SCONE* and *OpenSim* could account for the observed discrepancies, although this remained uncertain.

Additionally, the modelling of the wrist's degrees of freedom and contact points was simplified, leading to a shorter duration of push-off forces. Similarly, the contact point between the buttocks and the chair was simplified. The current modelling approach does not allow for a thigh roll-off when standing up, resulting in an abrupt decline in seat force rather than a gradual ascent.

Lastly, the validation of the AC strategy was limited. The simulation was compared only to joint moments and maximal muscle forces, while the other strategies were validated using kinematics, EMG, and environmental forces. The maximal muscle forces were also obtained through static optimization (SO), meaning they are simulated forces. A more comprehensive validation, similar to that used for the other strategies, was desired, but the experimental AC data collected has yet to be processed.

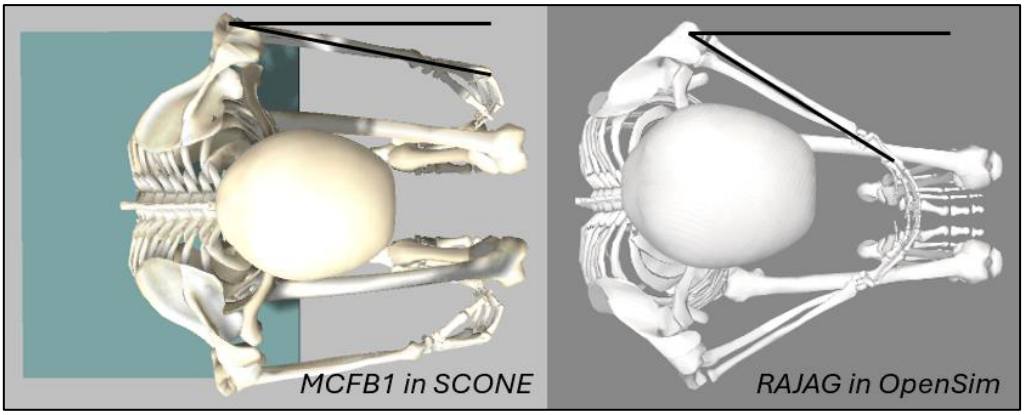

Figure 8: MCFB1 model in SCONE compared to the RAJAG model in OpenSim. Joint angles are the same between the models.

5.3: Recommendations

Considering these limitations, the study highlights several areas for future research. Currently, the model represents an average young male, yet experimental data has shown that movement can vary significantly, even within this demographic group. Expanding the model to include other demographic groups or personalized models could significantly enhance its application in clinical settings, helping to optimize individual movement strategies. The robustness of the current controller should be considered in this context. Testing the controller on models with different sizes, masses, and muscle strengths may provide insights into its robustness and help determine the next steps needed to improve its generality. Additionally, the effective use of the TP strategy under altered conditions suggests there may be additional, unrecognized benefits to this strategy. Further investigation into the TP strategy could reveal alternative advantages and potentially broaden its application. Additionally, further refinement of the contact points, specifically in the buttocks and wrists, may significantly improve the simulations in terms of environmental forces. Future studies should consider contacts allowing for roll-off, and additional dof's in the wrist. Finally, extending the simulation framework to predictively model the sit-to-stand-to-walk (STW) movement with arms – an area not yet studied – could also provide valuable insights into the integration of arm movements in other dynamic tasks.

References

[1] Dall, P. M., & Kerr, A. (2010). Frequency of the sit to stand task: An observational study of free-living adults. *Applied Ergonomics*, *41*(1), 58–61. https://doi.org/10.1016/j.apergo.2009.04.005

[2] Van Der Kruk, E., Silverman, A. K., Koizia, L., Reilly, P., Fertleman, M., & Bull, A. M. (2021). Age-related compensation: Neuromusculoskeletal capacity, reserve & movement objectives. *Journal Of Biomechanics*, *122*, 110385. https://doi.org/10.1016/j.jbiomech.2021.110385

[3] Fuller, G. F. (2000). Falls in the elderly. *PubMed*, *61*(7), 2159–4. https://pubmed.ncbi.nlm.nih.gov/10779256

[4] Van Der Kruk, E., Silverman, A. K., Reilly, P., & Bull, A. M. (2021). Compensation due to age-related decline in sit-to-stand and sit-to-walk. *Journal Of Biomechanics*, *122*, 110411. https://doi.org/10.1016/j.jbiomech.2021.110411

[5] Van Der Kruk, E., Strutton, P., Koizia, L. J., Fertleman, M., Reilly, P., & Bull, A. M. J. (2022). Why do older adults stand-up differently to young adults?: investigation of compensatory movement strategies in sit-to-walk. *Npj Aging*, *8*(1). https://doi.org/10.1038/s41514-022-00094-x

[6] De Groote, F., & Falisse, A. (2021). Perspective on musculoskeletal modelling and predictive simulations of human movement to assess the neuromechanics of gait. *Proceedings Of The Royal Society B: Biological Sciences*, *288*(1946), 20202432. https://doi.org/10.1098/rspb.2020.2432

[7] Van Der Kruk, E., & Geijtenbeek, T. (2024). A planar neuromuscular controller to simulate compensation strategies in the sit-to-walk movement. *PLoS ONE*, 19(6), e0305328. https://doi.org/10.1371/journal.pone.0305328

[8] Geyer, H., & Herr, H. (2010). A Muscle-Reflex Model That Encodes Principles of Legged Mechanics Produces Human Walking Dynamics and Muscle Activities. *IEEE Transactions On Neural Systems And Rehabilitation Engineering*, *18*(3), 263–273. https://doi.org/10.1109/tnsre.2010.2047592

[9] Muñoz, D., De Marchis, C., Gizzi, L., & Severini, G. (2022). Predictive simulation of sit-to-stand based on reflexive-controllers. *PLoS ONE*, *17*(12), e0279300. https://doi.org/10.1371/journal.pone.0279300

[10] Van Minnen, K. S. (2024). A 3D Neuromusculoskeletal Model with Reflex-Based Controllers for Predictive Simulation of the Sit-to-Stand Motion of Unilateral Transfemoral Amputees. [Master's thesis, Delft University of Technology]. *TUD Repository*

[11] Mazzà, C., Benvenuti, F., Bimbi, C., & Stanhope, S. J. (2004). Association Between Subject Functional Status, Seat Height, and Movement Strategy in Sit-to-Stand Performance. *Journal Of The American Geriatrics Society*, *52*(10), 1750–1754. https://doi.org/10.1111/j.1532-5415.2004.52472.x

[12] Davidson, B. S., Judd, D. L., Thomas, A. C., Mizner, R. L., Eckhoff, D. G., & Stevens-Lapsley, J. E. (2013). Muscle activation and coactivation during five-time-sit-to-stand movement in patients undergoing total knee arthroplasty. *Journal Of Electromyography And Kinesiology*, 23(6), 1485–1493. https://doi.org/10.1016/j.jelekin.2013.06.008

[13] Scarborough, D. M., McGibbon, C. A., & Krebs, D. E. (2007). Chair rise strategies in older adults with functional limitations. *The Journal Of Rehabilitation Research And Development*, *44*(1), 33. https://doi.org/10.1682/jrrd.2005.08.0134

[14] Komaris, D., Govind, C., Murphy, A., Ewen, A., & Riches, P. (2018). Identification of Movement Strategies During the Sit-to-Walk Movement in Patients With Knee Osteoarthritis. *Journal Of Applied Biomechanics*, *34*(2), 96–103. https://doi.org/10.1123/jab.2016-0279

[15] Van Der Kruk, E., & Geijtenbeek, T. (2024a). Is increased trunk flexion in standing up related to muscle weakness or pain avoidance in individuals with unilateral knee pain; a simulation study. *Frontiers in Bioengineering And Biotechnology*, *12*. https://doi.org/10.3389/fbioe.2024.1346365

[16] Hendriksen, M. C. (2021). Musculoskeletal Modelling of Three Sit-to-Stand Strategies in Elderly People. [Master's thesis, Delft University of Technology]. *TUD Repository*

[17] Dielissen, T.J. (2023). Evaluating the influence of different sit-to- stand strategies on the biomechanics of the upper extremity dependent on age and sex. [Master's thesis, Delft University of Technology]. *TUD Repository*

[18] Seth, A., Dong, M., Matias, R., & Delp, S. (2019). Muscle Contributions to Upper-Extremity Movement and Work From a Musculoskeletal Model of the Human Shoulder. *Frontiers in Neurorobotics*, *13*. https://doi.org/10.3389/fnbot.2019.00090

[19] Van Der Helm, F. (1994). Analysis of the kinematic and dynamic behavior of the shoulder mechanism. *Journal Of Biomechanics*, *27*(5), 527–550. https://doi.org/10.1016/0021-9290(94)90064-7

[20] Saul, K. R., Hu, X., Goehler, C. M., Vidt, M. E., Daly, M., Velisar, A., & Murray, W. M. (2014). Benchmarking of dynamic simulation predictions in two software platforms using an upper limb musculoskeletal model. *Computer Methods in Biomechanics & Biomedical Engineering*, *18*(13), 1445–1458. https://doi.org/10.1080/10255842.2014.916698

[21] Geijtenbeek T. https://hyfydy.com/. HyfyDy.

[22] Geijtenbeek, T. (2019). SCONE: Open Source Software for Predictive Simulation of Biological Motion. *The Journal Of Open Source Software*, *4*(38), 1421. https://doi.org/10.21105/joss.01421

[23] Millard, M., Uchida, T. K., Seth, A., & Delp, S. L. (2013). Flexing Computational Muscle: Modeling and Simulation of Musculotendon Dynamics. *Journal Of Biomechanical Engineering*, *135*(2). https://doi.org/10.1115/1.4023390

[24] Delp, S., Loan, J., Hoy, M., Zajac, F., Topp, E., & Rosen, J. (1990). An interactive graphics-based model of the lower extremity to study orthopaedic surgical procedures. *IEEE Transactions On Biomedical Engineering*, *37*(8), 757–767. https://doi.org/10.1109/10.102791

[25] Rajagopal, A., Dembia, C. L., DeMers, M. S., Delp, D. D., Hicks, J. L., & Delp, S. L. (2016). Full-Body Musculoskeletal Model for Muscle-Driven Simulation of Human Gait. *IEEE Transactions On Biomedical Engineering*, *63*(10), 2068–2079. https://doi.org/10.1109/tbme.2016.2586891

[26] Hunt, K. H., & Crossley, F. R. E. (1975). Coefficient of Restitution Interpreted as Damping in Vibroimpact. *Journal Of Applied Mechanics*, *42*(2), 440–445.
https://doi.org/10.1115/1.3423596

[27] Wang, J. M., Hamner, S. R., Delp, S. L., & Koltun, V. (2012). Optimizing locomotion controllers using biologically-based actuators and objectives. *ACM Transactions On Graphics*, *31*(4), 1–11.
https://doi.org/10.1145/2185520.2185521

[28] Caruthers, E. J., Thompson, J. A., Chaudhari, A. M., Schmitt, L. C., Best, T. M., Saul, K. R., & Siston, R. A. (2016). Muscle Forces and Their Contributions to Vertical and Horizontal Acceleration of the Center of Mass During Sit-to-Stand Transfer in Young, Healthy Adults. *Journal Of Applied Biomechanics*, *32*(5), 487–503.
https://doi.org/10.1123/jab.2015-0291

[29] Etnyre, B., & Thomas, D. Q. (2007). Event Standardization of Sit-to-Stand Movements. *Physical Therapy*, *87*(12), 1651–1666.
https://doi.org/10.2522/ptj.20060378

[30] Kera, T., Kawai, H., Takahashi, J., Hirano, H., Watanabe, Y., Fujiwara, Y., Ihara, K., Kim, H., & Obuchi, S. (2020). Association between ground reaction force in sit-to-stand motion and falls in community-dwelling older Japanese individuals. *Archives Of Gerontology And Geriatrics*, *91*, 104221.
https://doi.org/10.1016/j.archger.2020.104221

[31] Júdice, P. B., Hamilton, M. T., Sardinha, L. B., Zderic, T. W., & Silva, A. M. (2015). What is the metabolic and energy cost of sitting, standing and sit/stand transitions? *European Journal Of Applied Physiology*, *116*(2), 263–273.
https://doi.org/10.1007/s00421-015-3279-5

[32] Zhang, L., Liu, G., Han, B., Wang, Z., Yan, Y., Ma, J., & Wei, P. (2020). Knee Joint Biomechanics in Physiological Conditions and How Pathologies Can Affect It: A Systematic Review. *Applied Bionics And Biomechanics*, *2020*, 1–22.
https://doi.org/10.1155/2020/7451683

[33] Wu, G., Van Der Helm, F. C., Veeger, H., Makhsous, M., Van Roy, P., Anglin, C., Nagels, J., Karduna, A. R., McQuade, K., Wang, X., Werner, F. W., & Buchholz, B. (2005). ISB recommendation on definitions of joint coordinate systems of various joints for the reporting of human joint motion—Part II: shoulder, elbow, wrist and hand. *Journal Of Biomechanics*, *38*(5), 981–992.
https://doi.org/10.1016/j.jbiomech.2004.05.042

Appendix A: Muscle parameters + sources

Table A1: Lower limb muscle properties from Van der Kruk and Geijtenbeek (2024) [7], with changed maximal isometric force according to optimal fiber length / tendon slack length ratio from Delp et al. (1990) [18]

Lower limb:	Maximal isometric force, Delp et al. (1990) [18] (N)	Optimal fiber length, Delp et al. (1990) [18] (m)	Ratio (N/m)	Optimal fiber length, Van der Kruk et al. (2024) [7] (m)	Ratio * Optimal fiber length *MCFB1* (N)	Maximal isometric force thesis (N)
GMED1	819	0.078	10500	0.0733	766.5	1999
GMED2	573	0.0845	6781		495.0	
GMED3	653	0.0646	10108		737.9	
AMAG	1212	0.113	10726	0.087	1544	1544
ILIAC	1073	0.1	10730	0.1066	1148	1148
PSOAS	1113	0.1	11130	0.1169	1302	1302
GMAX SUP	573	0.142	4035	0.147	593.2	2108
GMAX MID	819	0.147	5571		874.7	
GMAX INF	552	0.144	3833		640.2	
HAM BIC	896	0.109	8220	0.0976	805.6	2310
HAM SEMI	1288	0.08	16100		1111	
HAM SEMT	410	0.201	2040		393.7	
BFSH	804	0.173	4647	0.1103	511.2	511.2
RF	1169	0.114	10254	0.114	1169	1169
VAS INT	1365	0.087	15690	0.0993	1553	5169
VAS LAT	1871	0.084	22274		2205	
VAS MED	1294	0.089	14539		1410	
GAS LAT	683	0.064	10672	0.051	629.6	1954
GAS MED	1558	0.06	25967		1324	
SOL	3549	0.05	70980	0.05	3123.12	3123
TA	905	0.098	9235	0.098	905	905

Table A2: Upper limb muscle properties with source and special notes

Upper limb:	Maximal isometric force (N)	Optimal Fiber Length (m)	Tendon slack length (m)	Pennation angle (rad)	Source	Special notes
CORB	208.2	0.0932	0.08	0.471239	Saul et al. (2015) [20]	Changed tendon slack length to reflect fiber + tendon Delp (2019)
TRIL	771.8	0.134	0.19	0.20944	Saul et al. (2015) [20]	Changed tendon slack length to reflect fiber + tendon Delp
TRILH	1435	0.1138	0.098	0.15708	Saul et al. (2015) [20]	Changed tendon slack length to reflect fiber + tendon Delp
BICL	525.1	0.1157	0.285	0	Saul et al. (2015) [20]	Changed tendon slack length to reflect fiber + tendon Delp
BICB	316.8	0.1321	0.1923	0	Saul et al. (2015) [20]	Changed tendon slack length to reflect fiber + tendon Delp
BRACH	1177.37	0.0858	0.0535	0	Saul et al. (2015) [20]	
DEL1	707.7	0.094	0.086	0.0872665	Delp et al. (2019) [18]	Deltoideus - Clavicle
DEL2	1324.4	0.0949	0.072	0.0872665	Delp et al. (2019) [18]	Deltoideus - Scapula
DEL3	2597.8	0.0748	0.065	0.0872665	Delp et al. (2019) [18]	Deltoideus - Scapula M
LATD	786.8	0.2656	0.0945	0	Delp et al. (2019) [18]	Maximal isometric force from combined Latissimus Dorsi S, M and I, Optimal fiber and tendon slack from Latissimus Dorsi M
PECM1	571.2	0.183	0.043	0	Delp et al. (2019) [18]	Pectoralis Major - Thorax
PECM2	683.2	0.15	0.026	0	Delp et al. (2019) [18]	Pectoralis Major M - Thorax
TERM	851.2	0.121	0.026	0	Delp et al. (2019) [18]	0.02 m from optimal fiber length to tendon slack length
SUPR	869.4	0.0591	0.064	0	Delp et al. (2019) [18]	Maximal isometric force from combined Supraspinatus P and A, Optimal fiber from Supraspinatus P, tendon slack length + 0.041 m

Table A3: Muscle properties of lower limbs

Lower limb:	Maximal isometric force (N)	Optimal Fiber Length (m)	Tendon slack length (m)	Pennation angle (rad)
GMED	1999	0.0733	0.066	0.3578
AMAG	1544	0.087	0.06	0.0872665
ILIAC	1148	0.1066	0.0934	0.279914
PSOAS	1302	0.1169	0.197	0.215525
GMAX	2108	0.147	0.127	0
HAM	2310	0.0976	0.325	0.202458
BFSH	511.2	0.1103	0.1	0.214675
RF	1169	0.114	0.305	0.0872665
VAS	5169	0.0993	0.123	0.0631
GAS	1954	0.051	0.39	0.172788
SOL	3123	0.05	0.25	0.436332
TA	905	0.098	0.223	0.0872665

Appendix B: Arm Swing Extensive Analysis

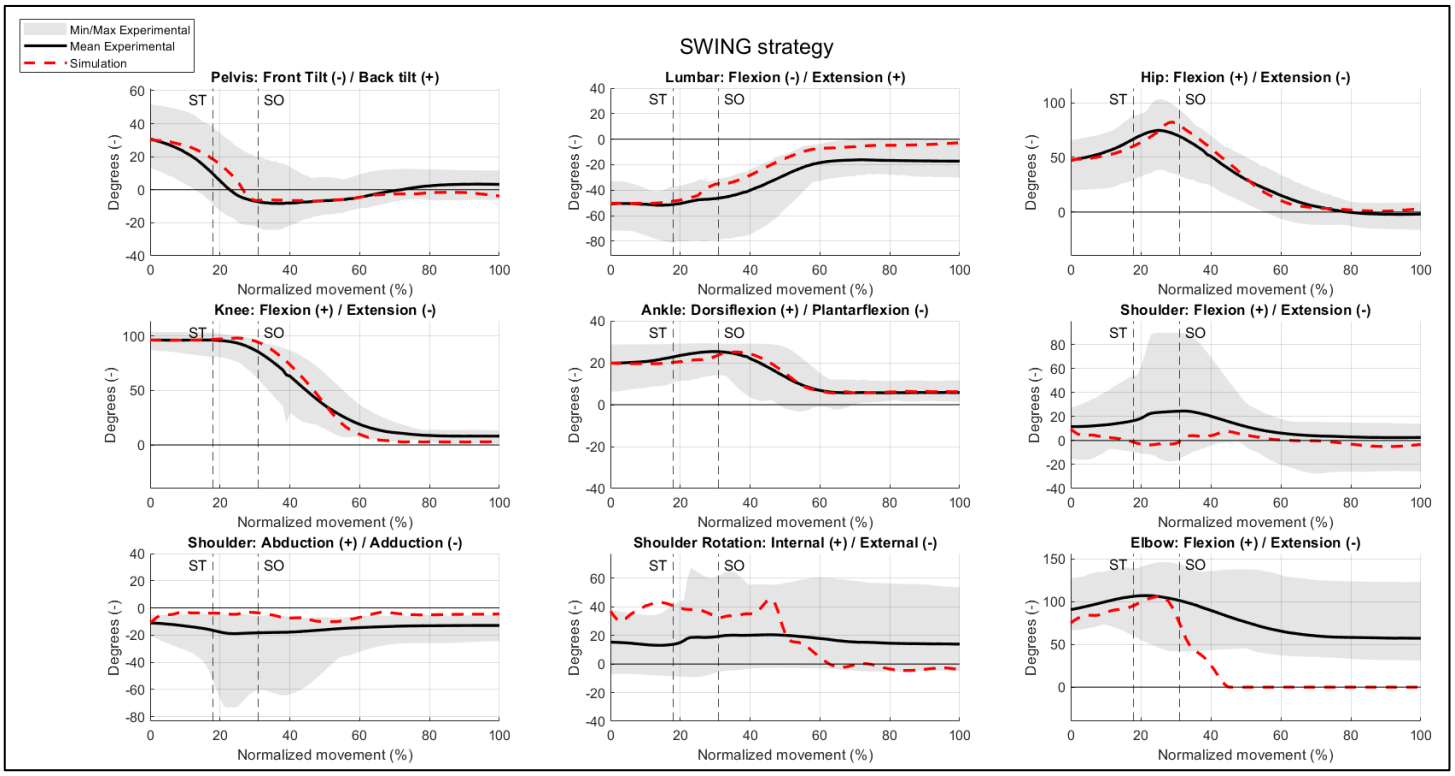

Figure B1: Right-sided joint angle verification between simulated and experimental joint angles for the arm swing strategy. Simulated angles shown as red striped line, mean experimental angles shown as black line with minimal and maximal range measured; Data was normalized over the duration of the STS movement. ST = State Transition, SO = Seat-Off

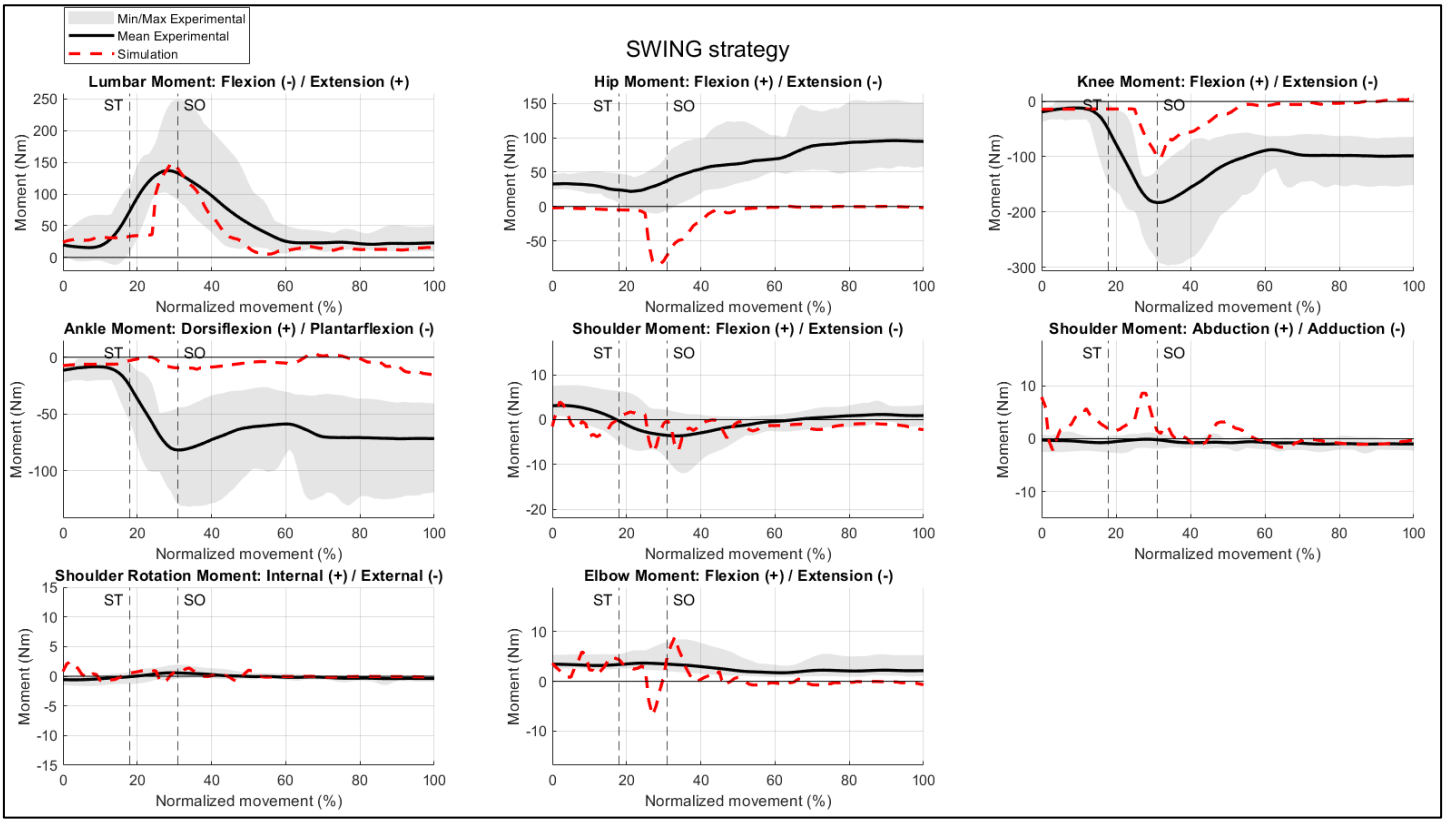

Figure B2: Right-sided joint moment verification between simulated and experimental joint moments for the arm swing strategy. Simulated moments shown as red striped line, mean experimental moments shown as black line with minimal and maximal moments range measured; Data was normalized over the duration of the STS movement. ST = State Transition, SO = Seat-Off

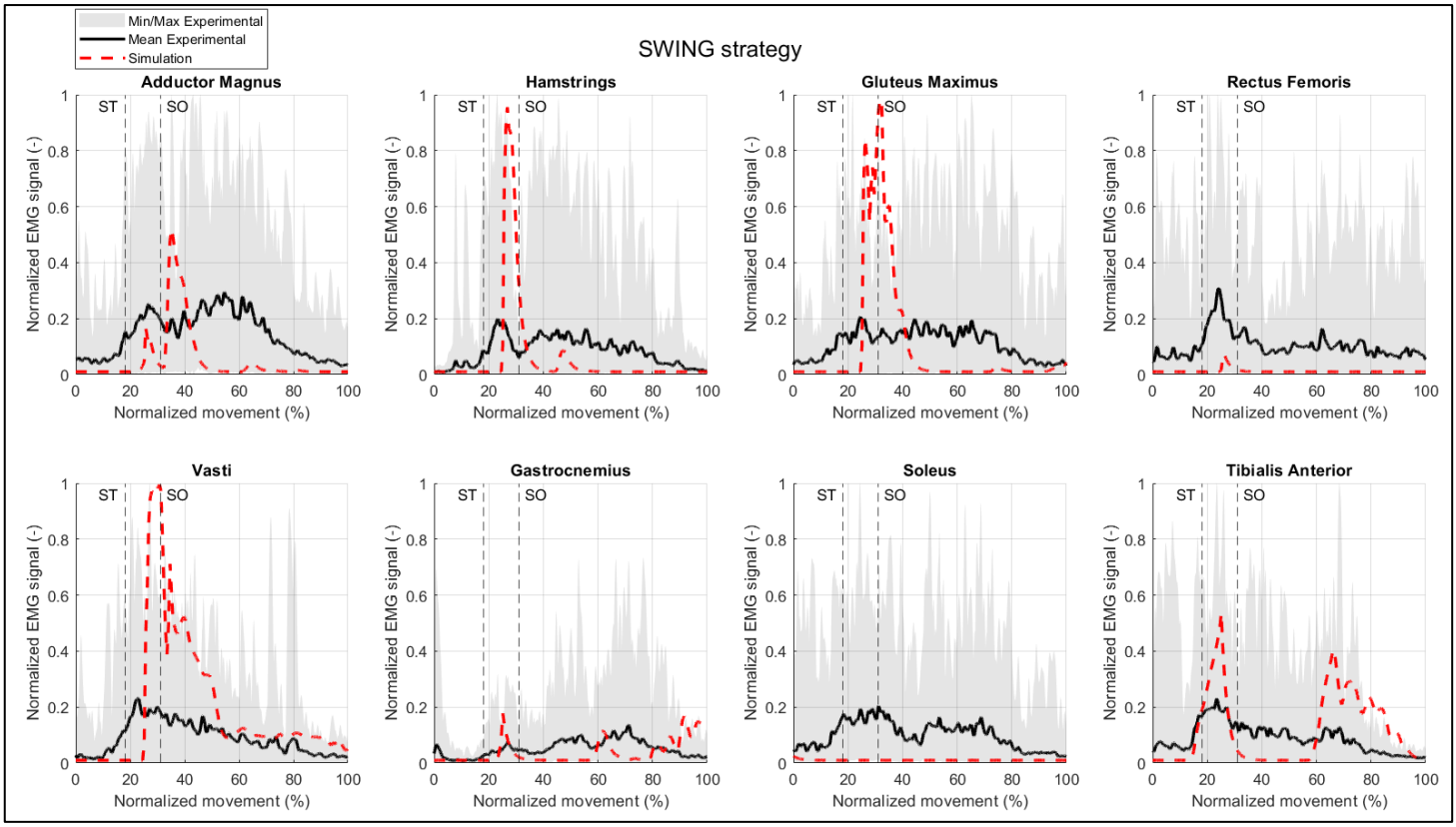

Figure B3: Right-sided muscle activation verification between simulated and experimental muscle activations for the arm swing strategy. Simulated activation shown as red striped line, mean EMG shown with minimal and maximal range measured. Data was normalized over the duration of the STS movement. ST = State Transition, SO = Seat-Off

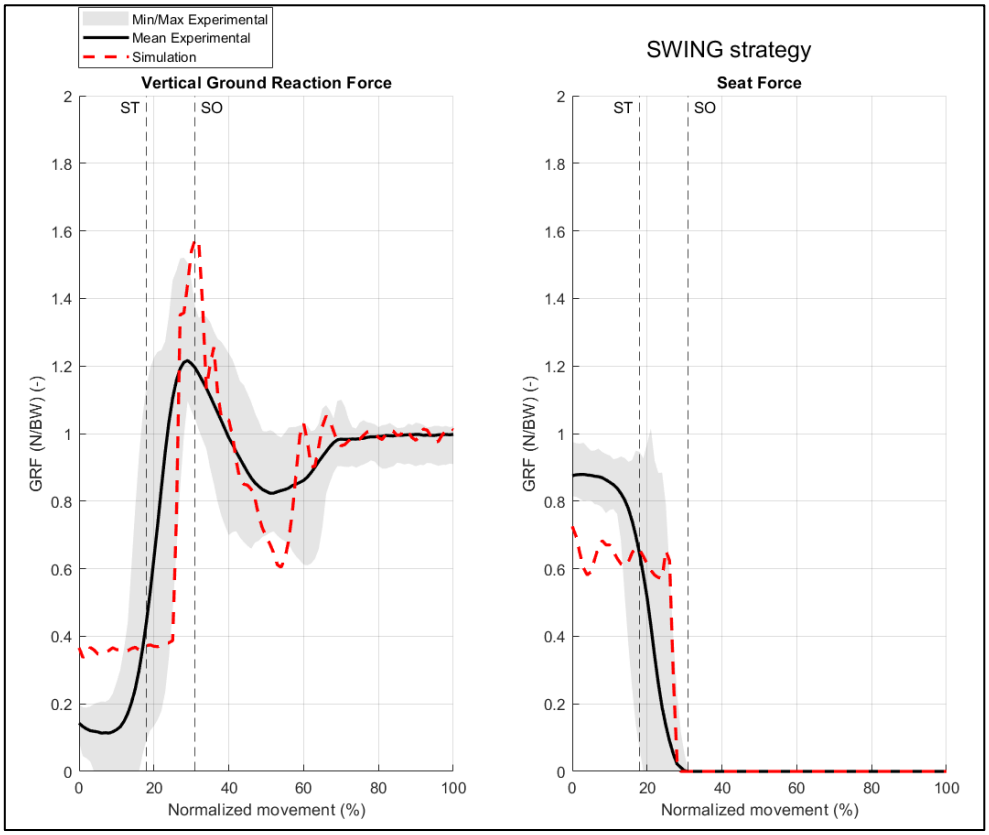

Figure 4: Environmental force verification between simulated and experimental forces for the arm swing strategy. Simulated force shown as red striped line, mean experimental force shown as black line with minimal and maximal range measured.; Data was normalized over the duration of the STS movement. ST = State Transition, SO = Seat-Off

Overall, the simulation of the arm swing strategy achieved comparable STS-kinematics compared to experimental data (Figure B1). Simulated angles apart from the elbow flexion displayed similar trends and fell within the range of motion of the experimental angles. The simulated elbow was extended while the experimental elbow showed flexion. The arm swing was underutilized in both the simulation and trials. Both showed moderate initial elbow flexion, and the mean measured shoulder only flexed slightly initially. Other arm angles were kept relatively constant. Experimental hip joint and ankle joint moments displayed irregularities compared to the other strategies (Figure B2). A hip joint extension moment was expected, but the measured data shows a hip flexion moment. Furthermore, the magnitude of the ankle plantarflexion moment was significantly higher compared to the other strategies (approximately peak of +100 Nm). The simulated AS hip joint extension moment was similar to the experimental AP and TP hip joint extension moments. The simulated knee extension moment was relatively lower compared to the experimental knee extension moment. The simulated shoulder portrayed abduction moment, while the measured moment was close to zero. Similarly, the simulated elbow showed elbow extension moment, where the experimental elbow moments showed a constant flexion moment. The simulated HAM, VAS and GMAX muscles showed generally high activations (Figure B3). The RF, SOL and GAS showed close to no activation in the simulation, while portraying activation in the EMG data. This may explain the low ankle joint moments, as almost all lower leg muscles were turned off. For the environmental forces (Figure B4), both the simulated and experimental GRF showed similar trends, also found by Etnyre et al. (2007) in all participants [29]. Difference was seen in the seat force between the simulation and the experiment. The modelling of the contact point between the buttocks and seat did not account for the roll-off from buttocks to thigh, leading to a more abrupt decline. Additionally, the maximum GRF was 0.4 N/BW higher in the simulation, potentially due to the high activations of the lower limb muscles, which generated greater knee and hip extension moments, and consequently, a larger downward push of the legs on the floor.

Appendix C: Armrest Push-off Extensive Analysis

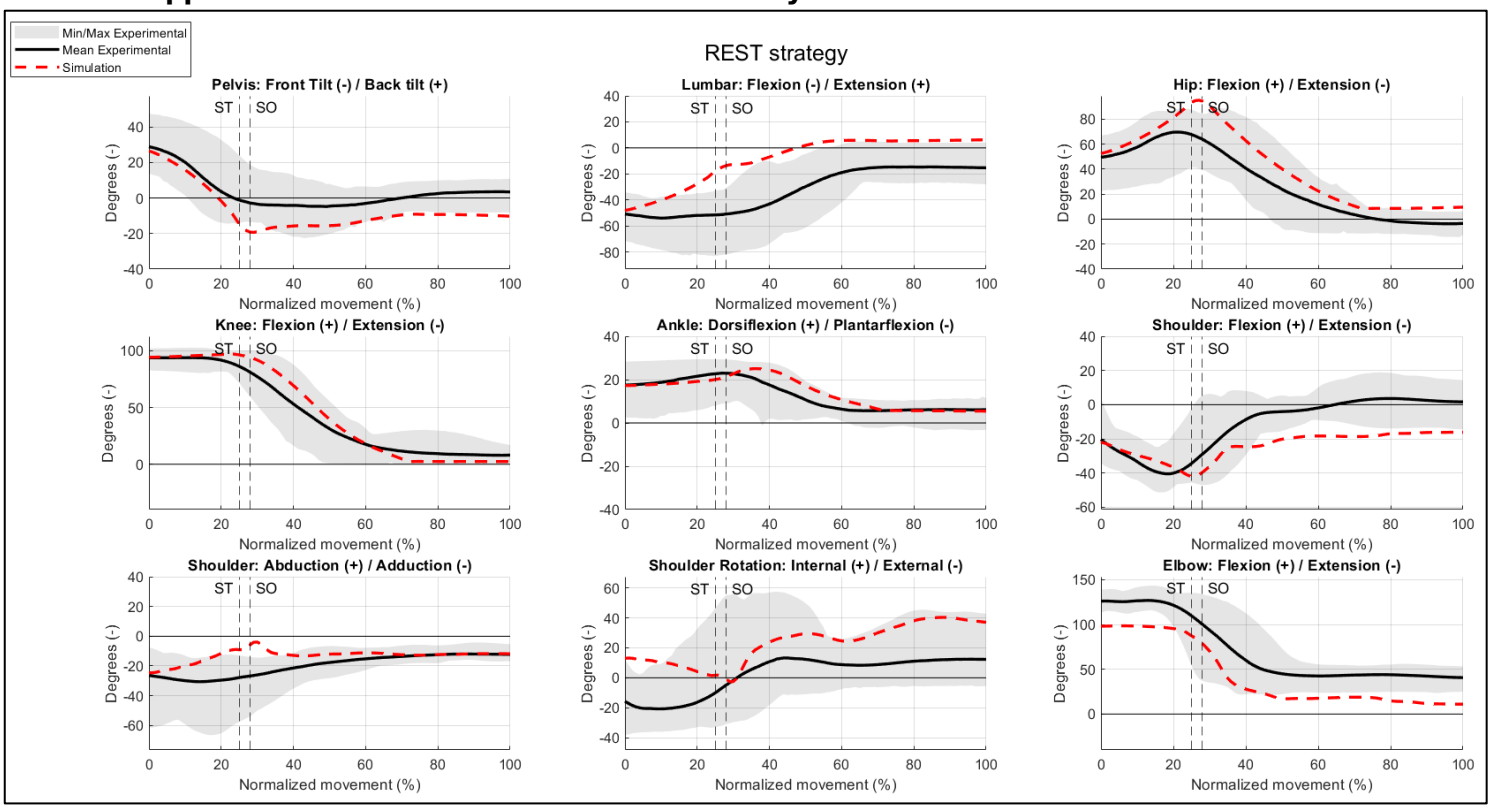

Figure C1: Right-sided joint angle verification between simulated and experimental joint angles for the armrest push-off strategy. Simulated angles shown as red striped line, mean experimental angles shown as black line with minimal and maximal range measured; Data was normalized over the duration of the STS movement. ST = State Transition, SO = Seat-Off

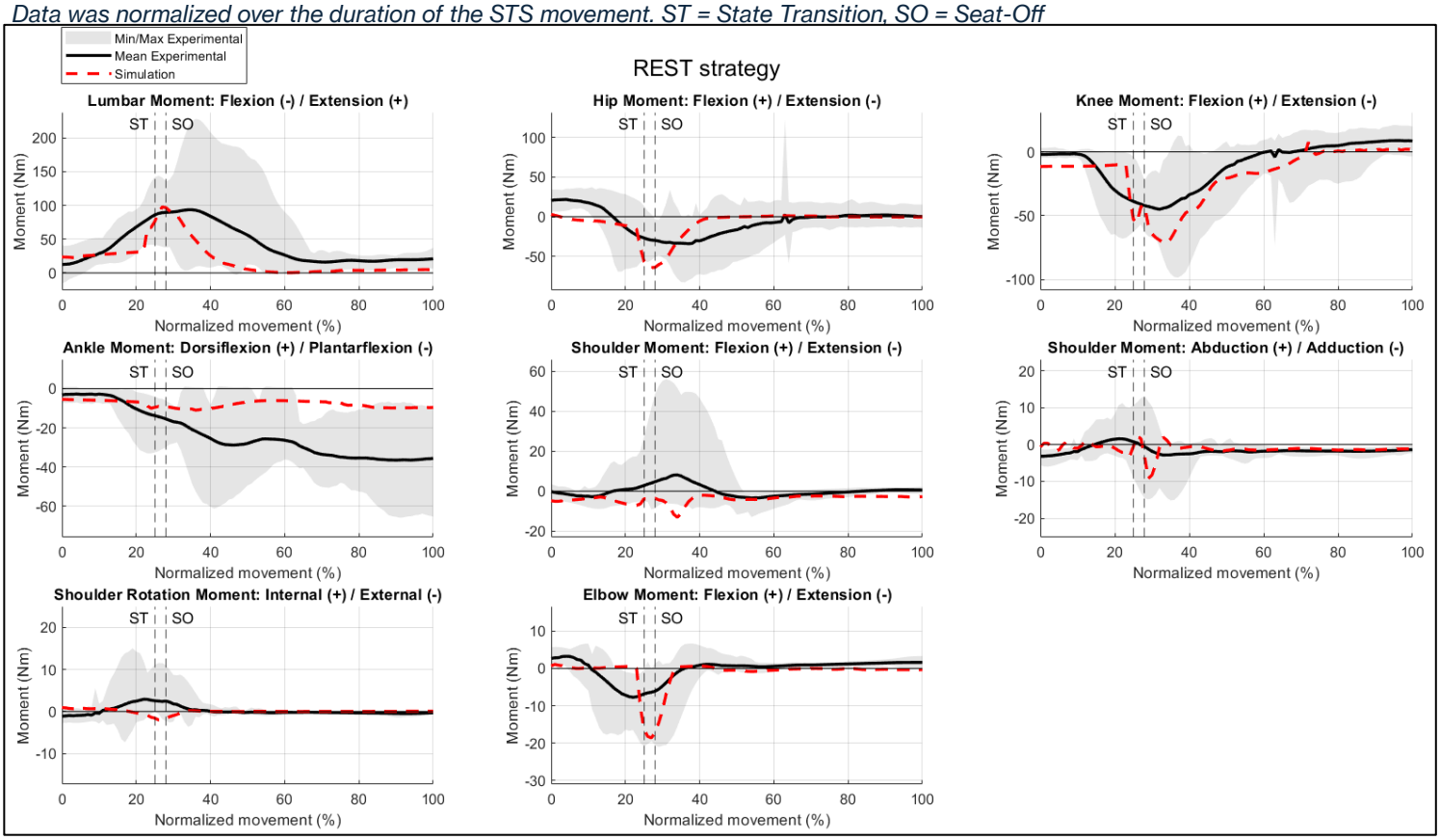

Figure C2: Right-sided joint moment verification between simulated and experimental joint moments for the armrest push-off strategy. Simulated moments shown as red striped line, mean experimental moments shown as black line with minimal and maximal range measured. Data was normalized over the duration of the STS movement. ST = State Transition, SO = Seat-Off

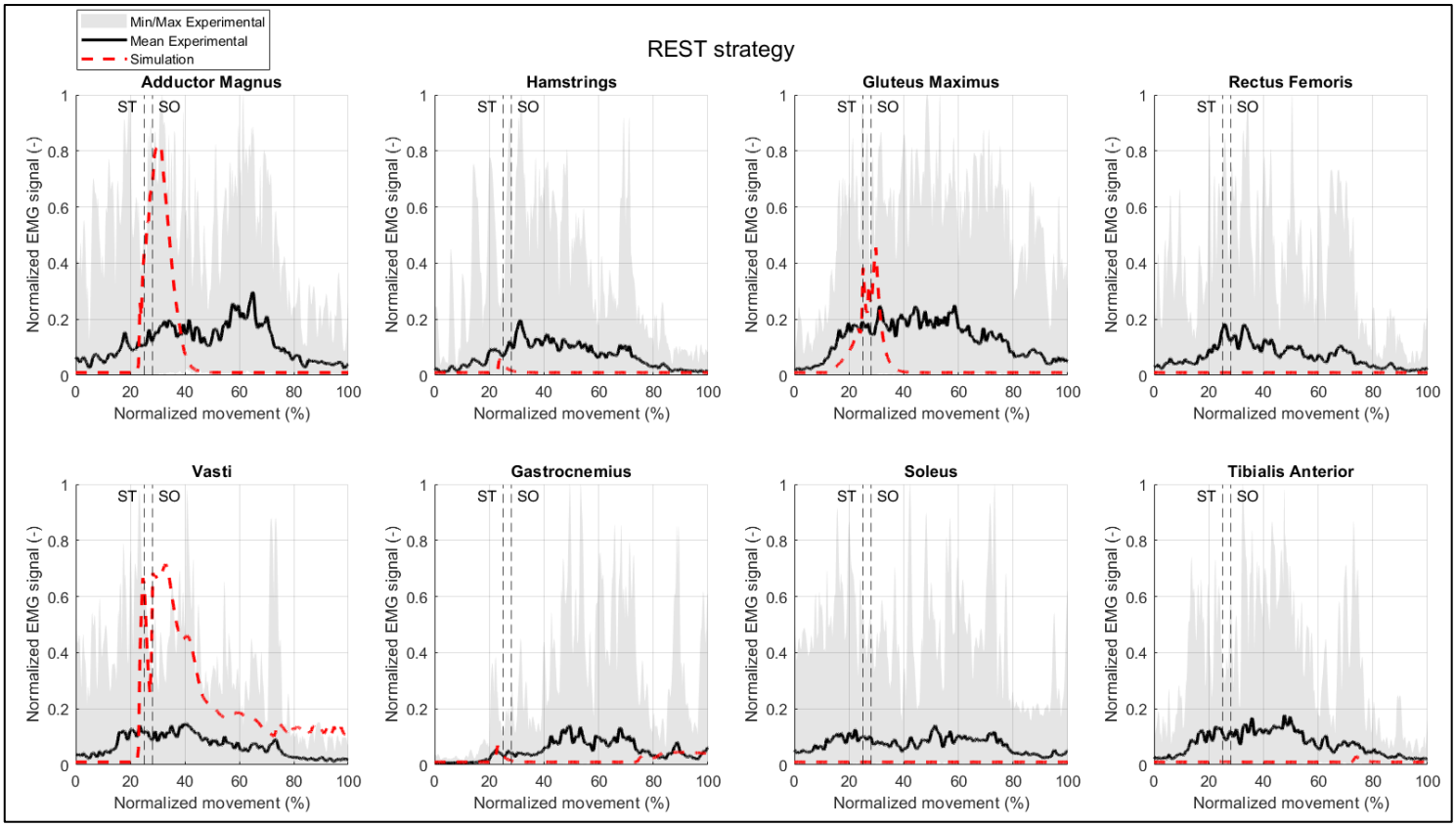

Figure C3: Right-sided muscle activation verification between simulated and experimental muscle activations for the armrest push-off strategy. Simulated activation shown as red striped line, experimental EMG shown as black line with minimal and maximal range measured; Data was normalized over the duration of the STS movement. ST = State Transition, SO = Seat-Off

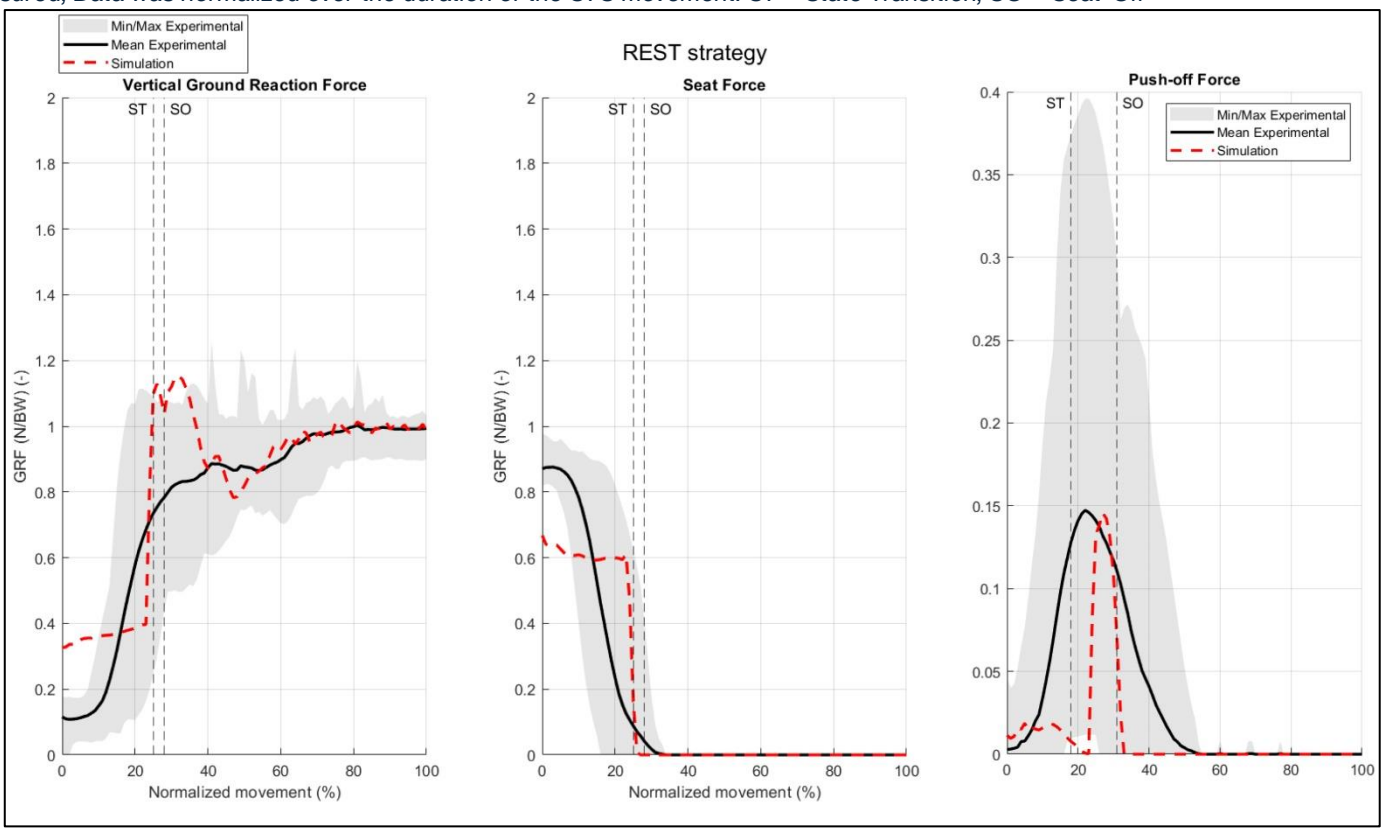

Figure C4: Environmental force verification between simulated and experimental forces for the arm swing strategy. Simulated force shown as red striped line, mean experimental force shown as black line with minimal and maximal range measured; Data was normalized over the duration of the STS movement.

Overall, the joint angles were relatively comparable between simulation and experiment (Figure C1). The pelvis tilt and lumbar extension in the simulation exhibited an offset compared to the measured motion. Additionally, the hip flexion at the end of the motion exceeded the bounds of the experimental data. Consistent with previous strategies, the shoulder rotation and elbow flexion in the simulation mirrored the trends in the experimental data but showed discrepancies of 30 degrees in overestimation and underestimation, respectively. For joint moments, the simulated moments fell within the measured range (Figure C2). The exception was the simulated ankle moment, showing overall lower magnitude of moment compared to the experimental data. The muscle activations showed generally lower activations compared to the other strategies (Figure C3). The AMAG and GMAX were turned off after their peak activation, while experimental data shows these muscles to be active during the latter part of the motion. The HAM, RF, GAS, SOL and TA all showed no activation in the simulation. This may explain the low ankle joint moments, as almost all lower leg muscles were turned off. In contrast to previous strategies, the experimental GRF did not exceed the 1 N/BW threshold when using the armrests (Figure C4). Utilizing the armrests facilitated a smoother balance shift from buttocks to feet, a transition that was not as fluid in the simulated data. The GRF peaked slightly above 1 N/BW, within the measured range. Figure C4 further illustrates the push-off force exerted by the hands on the armrests. The simulation showed a similar peak push-off force, but a shorter duration of force application compared to the experimental data.

Appendix D: Thigh Push-off Extensive Analysis

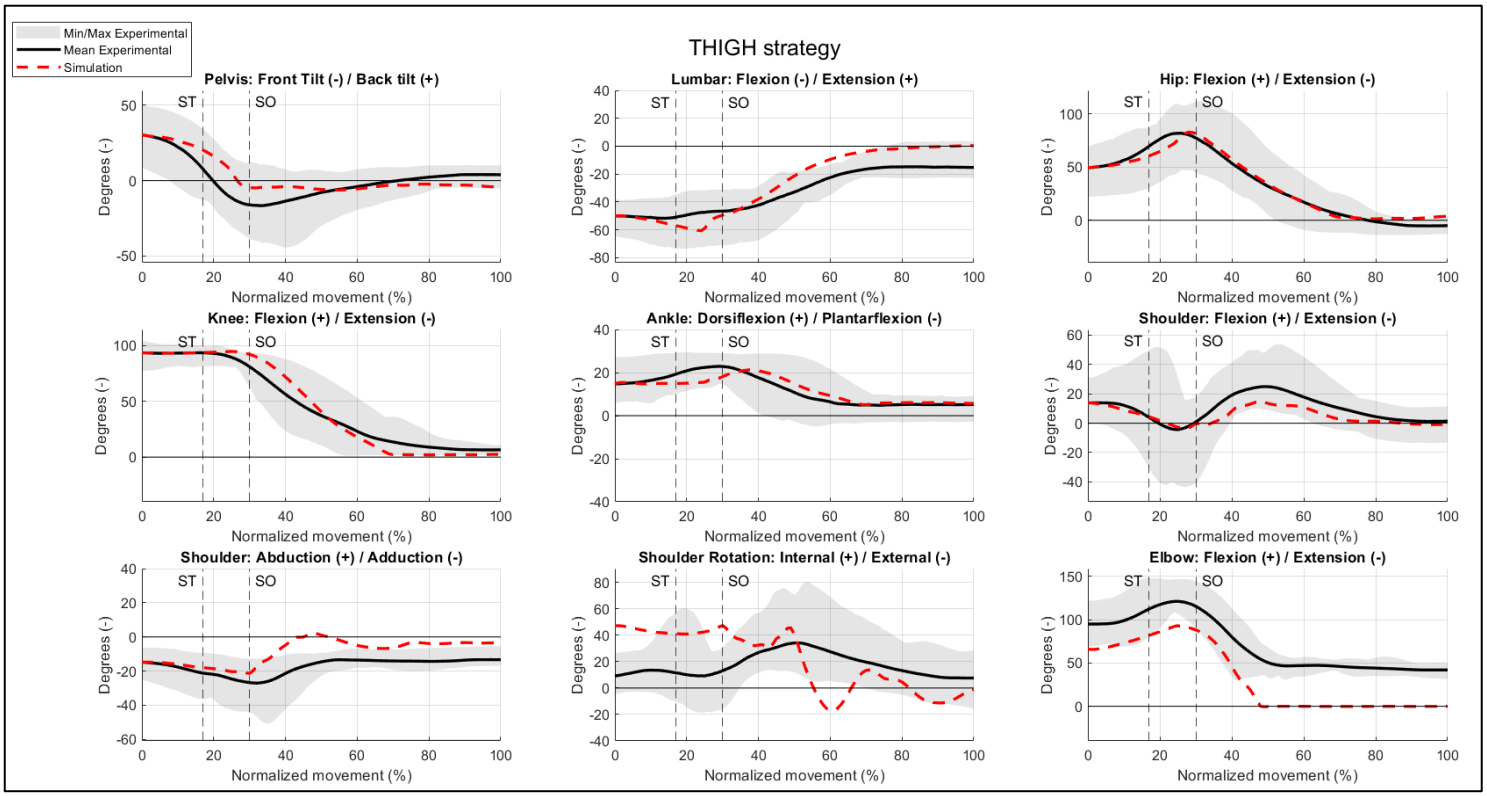

Figure D1: Right-sided joint angle verification between simulated and experimental joint angles for thigh push-off strategy. Simulated angles shown as red striped line, mean experimental angles shown as black line with minimal and maximal range of motion measured; Data was normalized over the duration of the STS movement. ST = State Transition, SO = Seat-Off

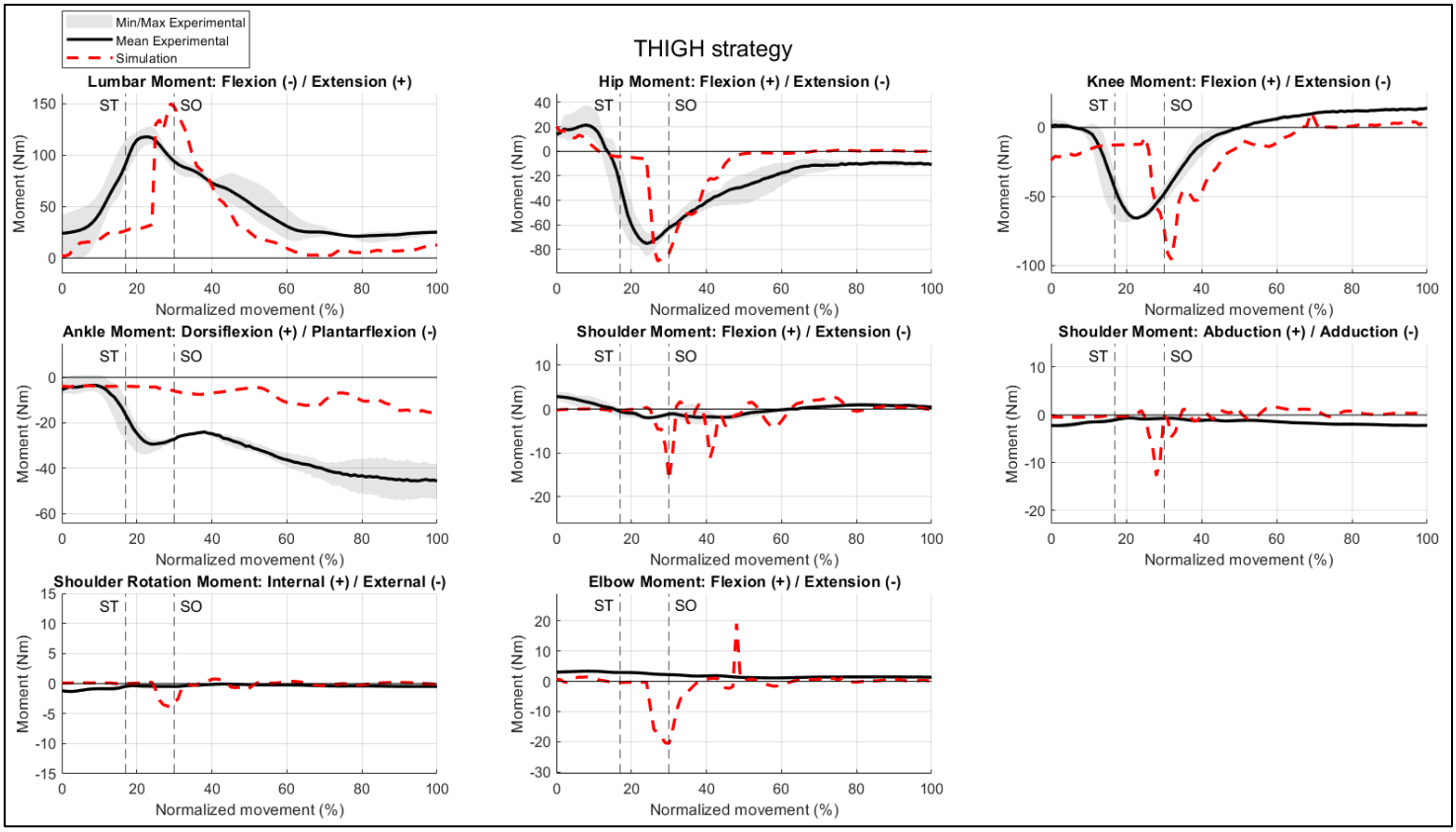

Figure D2: Right-sided joint moment verification between simulated and experimental joint moments for thigh push-off strategy. Simulated moments shown as red striped line, mean experimental moments shown as black line with minimal and maximal range measured; Data was normalized over the duration of the STS movement. ST = State Transition, SO = Seat-Off

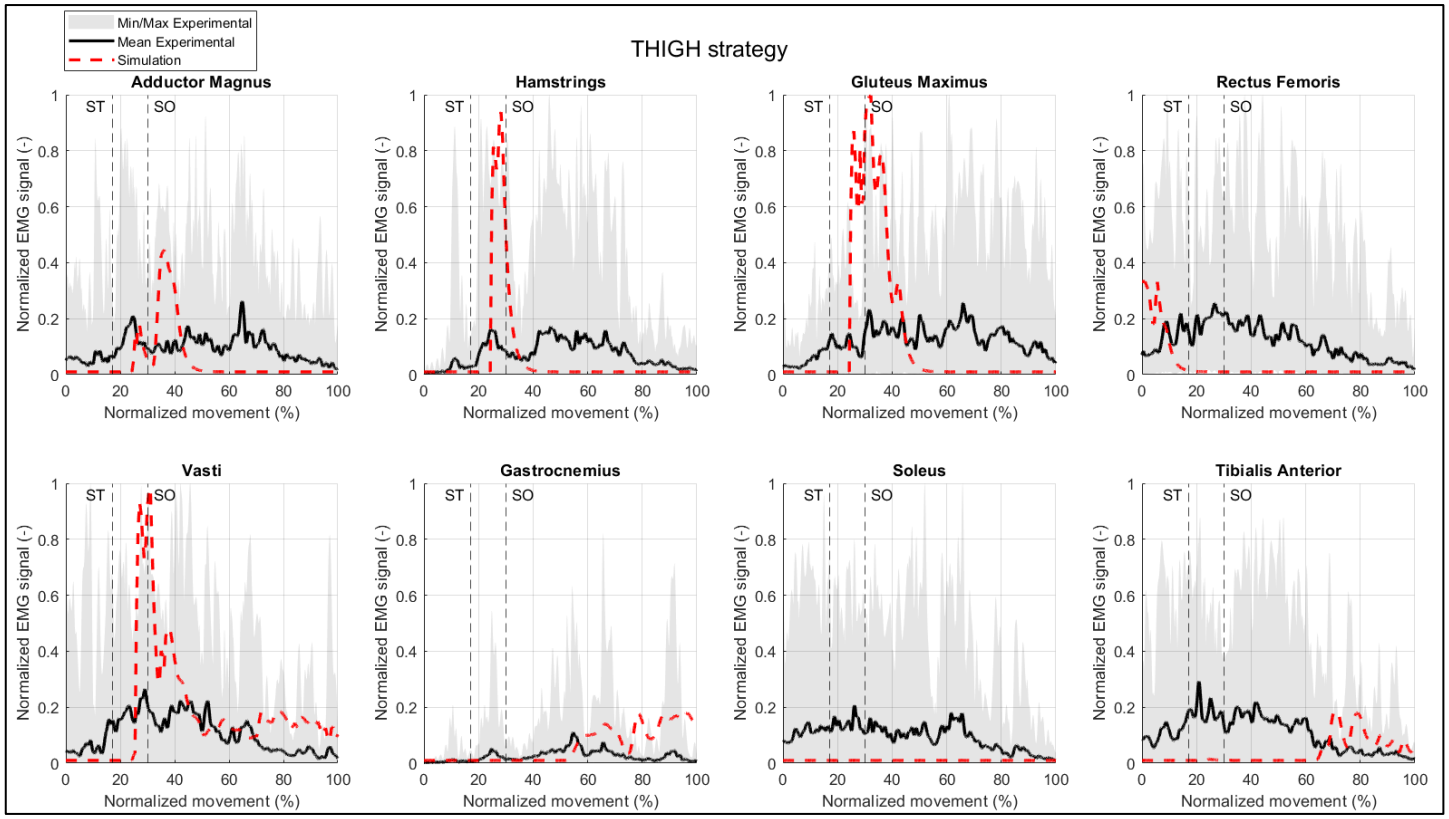

Figure D3: Right-sided muscle activation verification between simulated and experimental muscle activations for the thigh push-off strategy. Simulated activation shown as red striped line, experimental EMG shown as black line with minimal and maximal measured range; Data was normalized over the duration of the STS movement. ST = State Transition, SO = Seat-Off

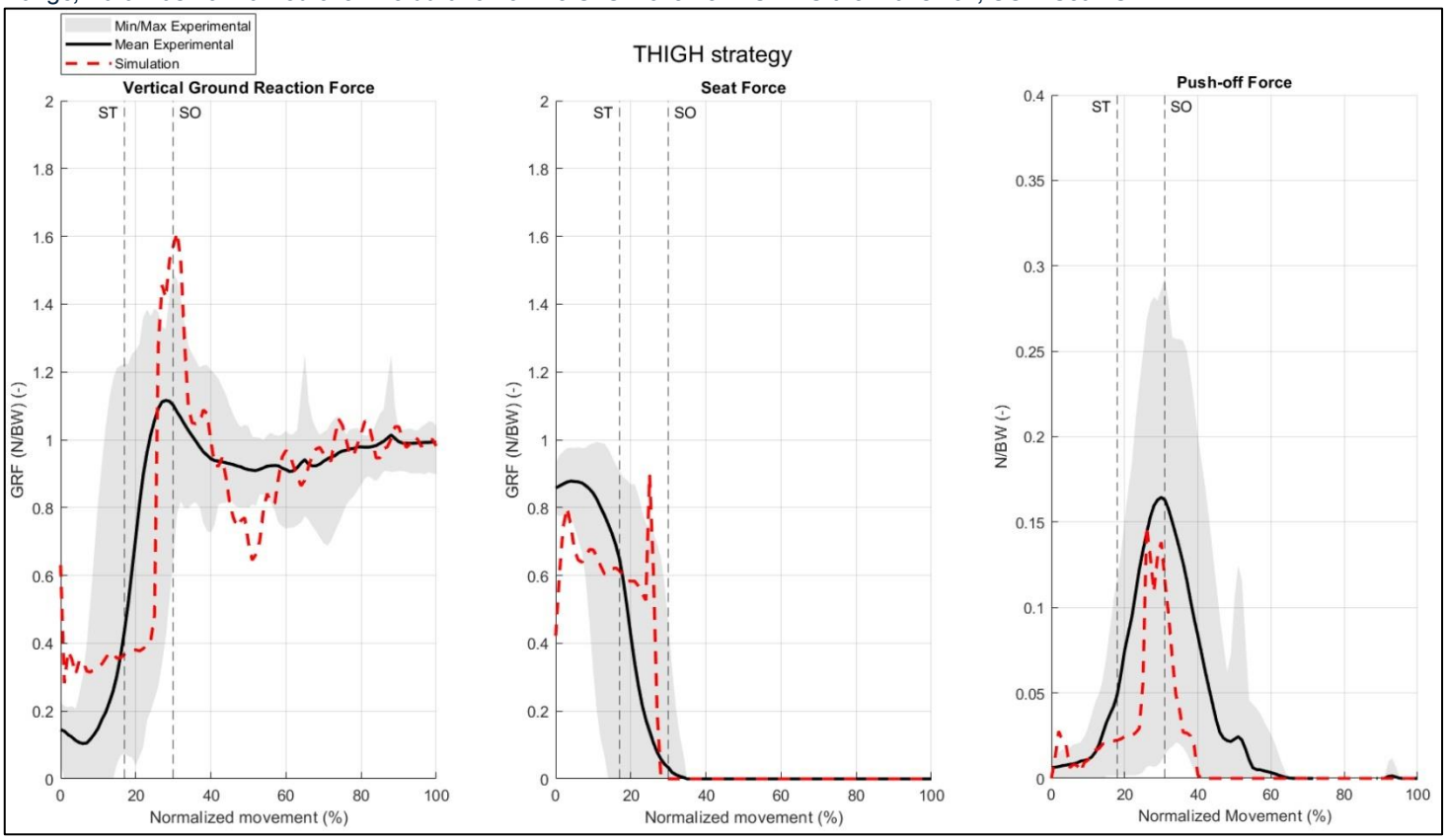

Figure D4: Environmental force verification between simulated and experimental forces for the arm swing strategy. Simulated force shown as red striped line, experimental force shown as black line with minimal and maximal range measured. Data was normalized over the duration of the STS movement. ST = State Transition, SO = Seat-Off

The simulation of the thigh push-off strategy achieved comparable STS-kinematics compared to experimental data (Figure D1). The simulated shoulder rotation and elbow flexion, while displaying similar trends, were over- and underestimated by approximately 30 degrees, respectively. Joint moments were comparable between simulation and experiment. Note the ranges of moments was smaller compared to the other strategies. Only three runs with acceptable data were available for the TP joint moments. The simulated ankle moment was underestimated, while the arm angles each displayed a peak near seat-off. This would be were the push-off moment was greatest. The experimental data did not show these peaks, but could be attributed to the fact the experimental runs used belonged to a single participant. The simulated HAM, VAS and GMAX muscles showed generally high activations (Figure D3). The RF, SOL, GAS and TA showed close to no activation in the simulation, while portraying activation in the EMG data. This may explain the low ankle joint moments, as almost all lower leg muscles were turned off. For the environmental forces (Figure D4), both the simulated and experimental GRF showed similar trends, also found by Etnyre et al. (2007) in all participants [29]. Difference was seen in the seat force between the simulation and the experiment. The modelling of the contact point between the buttocks and seat did not account for the roll-off from buttocks to thigh, leading to a more abrupt decline. Additionally, the maximum GRF was 0.3 N/BW higher in the simulation, potentially due to the high activations of the lower limb muscles, which generated greater knee and hip extension moments, and consequently, a larger downward push of the legs on the floor. Figure D4 additionally depicts the push-off force exerted by the hands on the thighs. The duration of force application was shorter in the simulation compared to the experimental data.

Appendix E: Arms Crossed Extensive Analysis

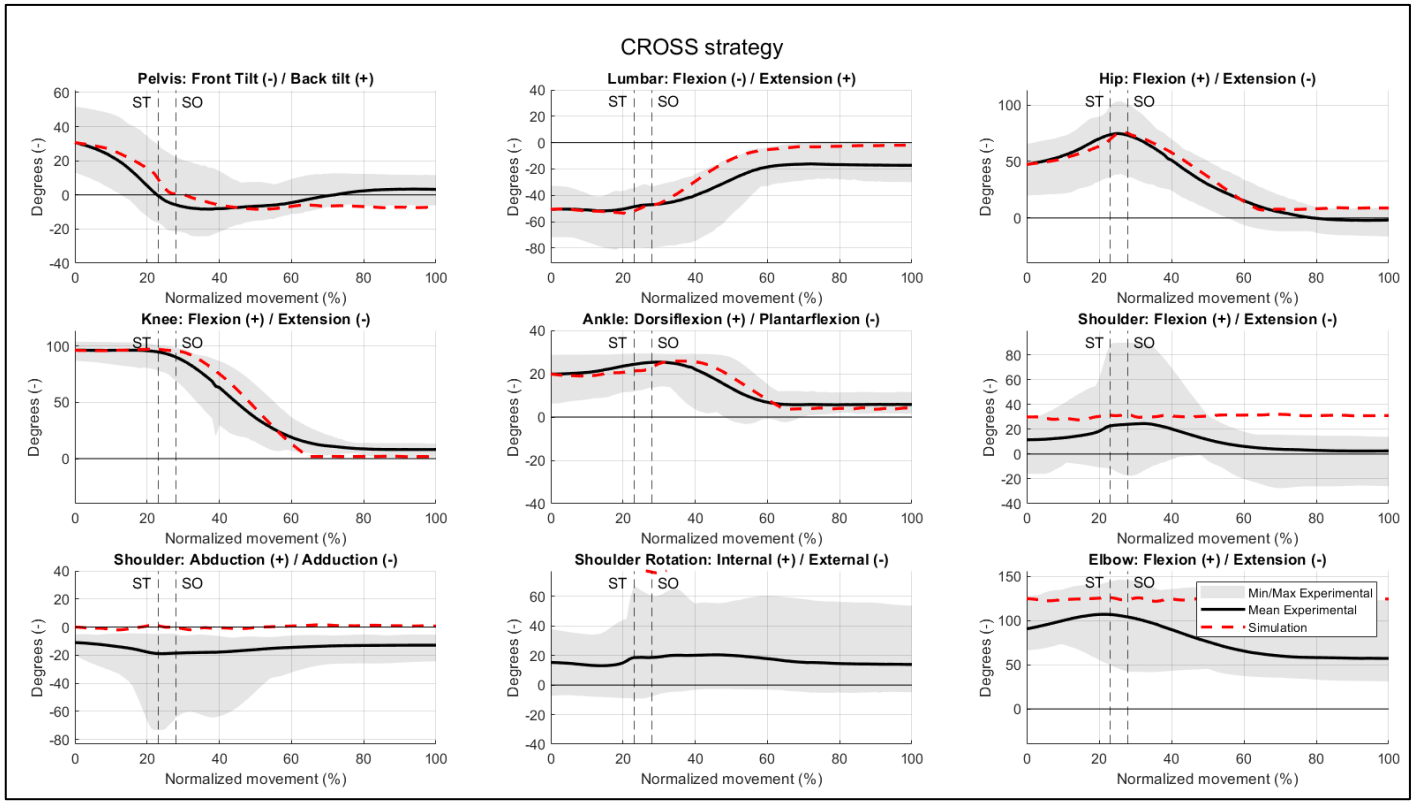

Figure E1: Right-sided joint angle verification between simulated arms crossed and experimental arm swing joint angles Simulated angles shown as red striped line, experimental angles shown as black line with minimal and maximal range measured; Data was normalized over the duration of the STS movement. ST = State Transition, SO = Seat-Off

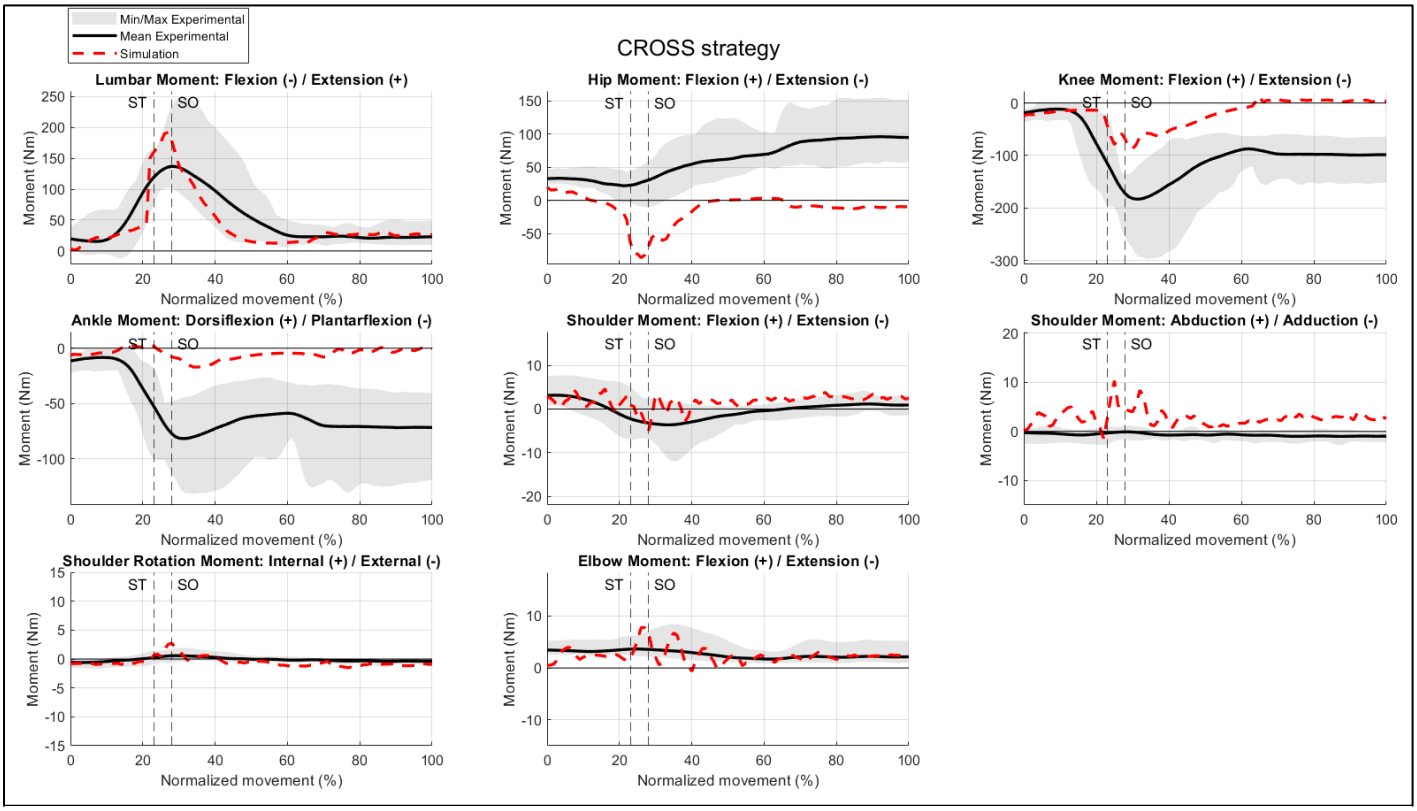

Figure E2: Right-sided joint moment verification between simulated arms crossed and experimental arm swing joint moments. Simulated moments shown as red striped line, mean experimental moments shown as black line with minimal and maximal measured range; Data was normalized over the duration of the STS movement. ST = State Transition, SO = Seat-Off

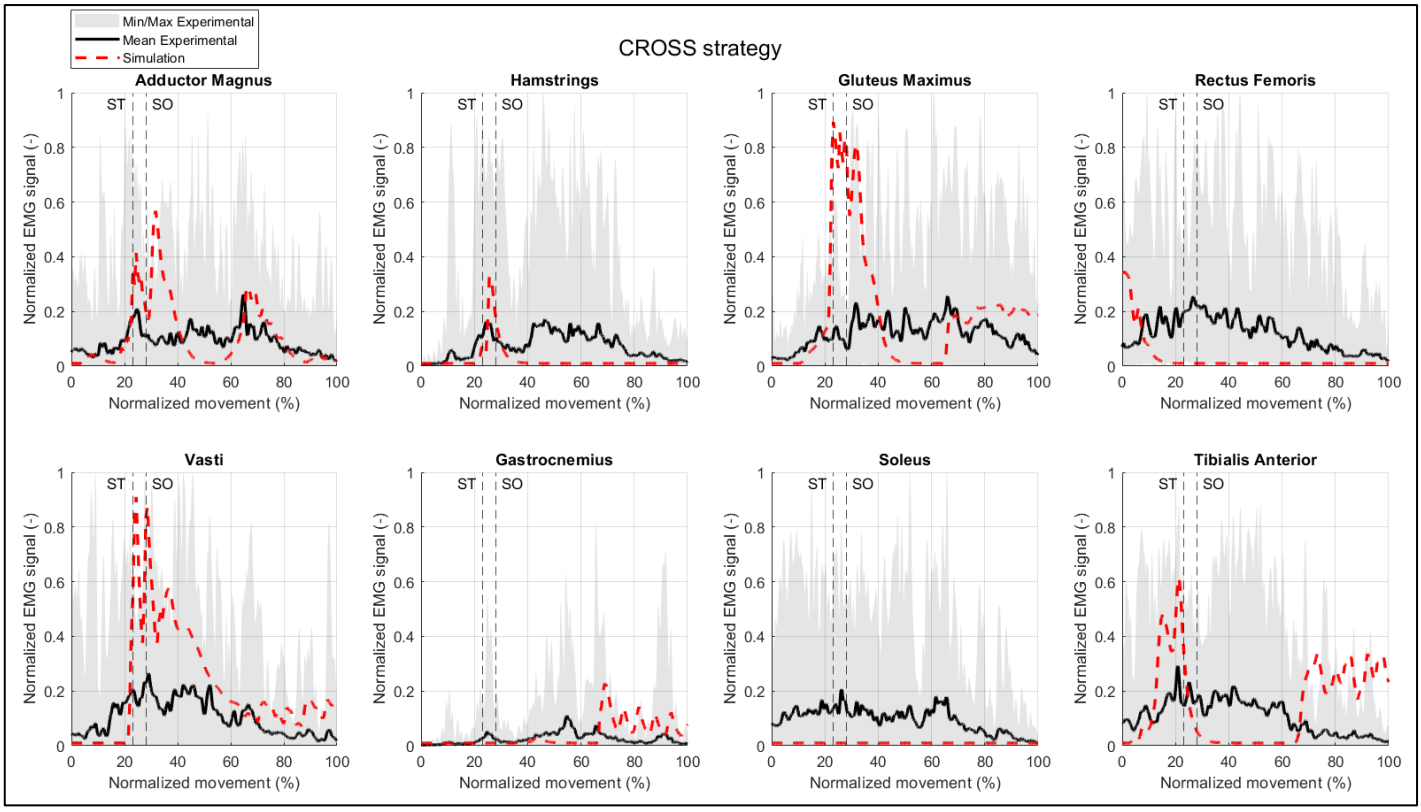

Figure E3: Right-sided muscle activation verification between simulated arms crossed and experimental arm swing muscle activations. Simulated activation shown as red striped line, mean experimental EMG as a black line with minimal and maximal measured range.. Data was normalized over the duration of the STS movement. ST = State Transition, SO = Seat-Off

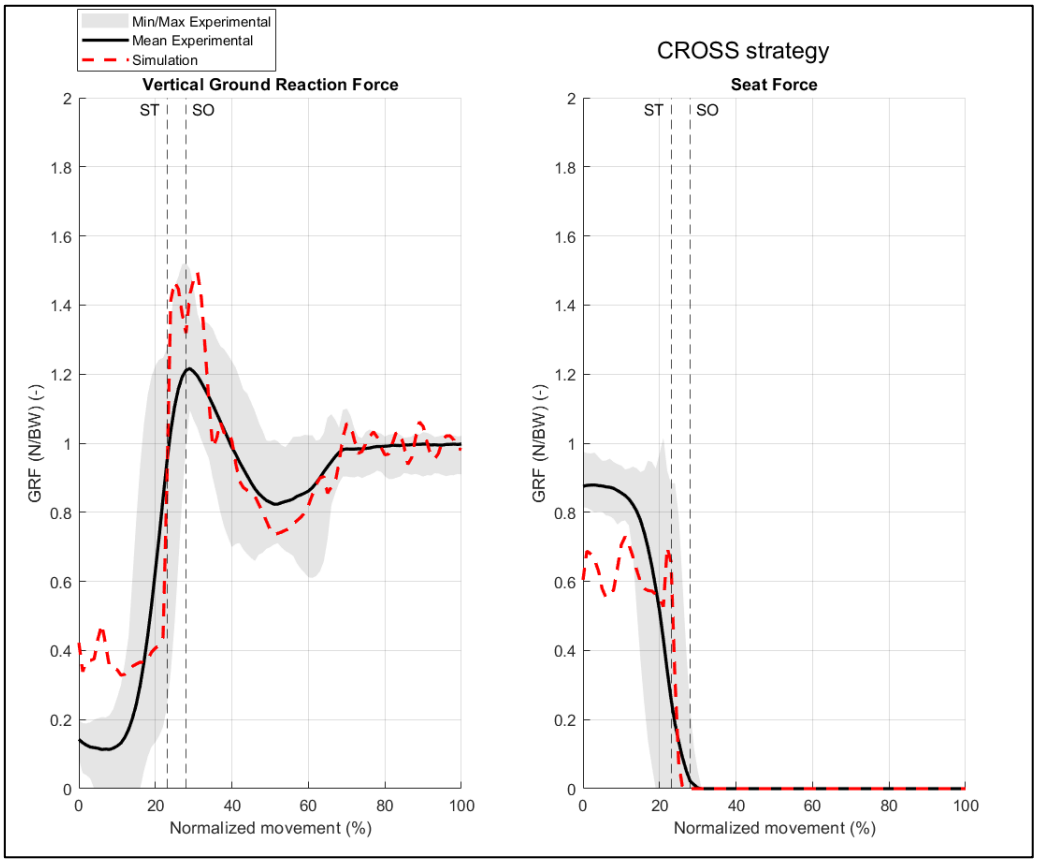

Figure E4: Environmental force verification between simulated arms crossed and experimental arm swing forces. Simulated force shown as red striped line, mean experimental force shown as black line with minimal and maximal measured range.; Data was normalized over the duration of the STS movement. ST = State Transition, SO = Seat-Off

The arms crossed (AC) strategy was not included in the experimental data used in this study. The simulation was therefore compared to the arms swing (AS) strategy. Lower limb kinematics, muscle activations and environmental forces should show relative similarities with the AS strategy. The upper limbs were excluded.

Overall, the simulation of the AC strategy achieved comparable lower limb STS-kinematics compared to experimental AS strategy (Figure E1). Simulated lower limb angles displayed similar trends and fell within the range of motion of the experimental angles. For the joint moments (Figure E2), the lumbar extension moment was similar between simulation and experiment. The simulated knee extension moment was relatively lower compared to the experimental knee extension moment. As mentioned in Appendix B, the AS experimental hip joint and ankle joint moments displayed irregularities compared to the other strategies. A hip joint extension moment was expected, but the measured data shows a hip flexion moment. Furthermore, the magnitude of the ankle plantarflexion moment was significantly higher compared to the other strategies (approximately peak of +100 Nm). The simulated AC hip joint extension moment was similar to the experimental AP and TP hip joint extension moments. The simulated VAS and GMAX muscles showed generally high activations (Figure E3). The HAM, SOL and GAS showed close to no activation in the simulation, while portraying activation in the EMG data. This may explain the low ankle joint moments, as almost all lower leg muscles were turned off. For the environmental forces (Figure E4), both the simulated and experimental GRF showed similar trends, also found by Etnyre et al. (2007) in all participants [29]. Difference was seen in the seat force between the simulation and the experiment. The modelling of the contact point between the buttocks and seat did not account for the roll-off from buttocks to thigh, leading to a more abrupt decline. Additionally, the maximum GRF was 0.2 N/BW higher in the simulation, potentially due to the increased activation of the VAS and GMAX muscles, which generated greater knee and hip extension moments, and consequently, a larger downward push of the legs on the floor. The vertical GRF did however fall within the maximal range measured.

Appendix F: Offset in shoulder rotation and elbow flexion

As seen for each strategy, the shoulder rotation and elbow flexions displayed similar trends to the experimental data, but at a seemingly offset of about 30 degrees. Figure F1 shows visually the differences between the arms of the *MCFB1* model in *SCONE,* and the *RAJAG* model used in the experimental data in *OpenSim*.